J-couplings. Measurement and Usage in Structure Determination

Dr. Geerten W. Vuister

Department of Biophysical Chemistry
University of Nijmegen
Toernooiveld 1
6525 ED Nijmegen, The Netherlands
http://www.nmr.kun.nl

Largely based upon:
G.W. Vuister et al., “Pulse Sequences for Measuring Coupling Constants” in Biological Magnetic Resonance, Vol. 16: Modern Techniques in Protein NMR, edited by Krishna and Berliner, Kluwer Academic/Plenum Publishers, 1998.
Updated: July 2002, August 2003

Contents

1. Introduction

It has been recognized since the early days of NMR that the J-coupling constants contain very useful information regarding molecular conformation (Karplus, 1959, 1963; Bystrov, 1976). For small (bio)molecules the magnitude of the J-coupling constants can often be measured directly from the splitting of the resonances of interest. However, the accurate measurement of the magnitude of the J-coupling constants has been problematic for larger biomolecules in which the measurements of in-phase or antiphase splittings failed.

With the recent advent of isotope labeling techniques in proteins, RNA, and DNA molecules interest in the measurement of J-couplings has again surged. The usage of isotope labels has prompted the development of a series of experiments aimed at measuring a large array of both homo- and heteronuclear coupling constants. As a result of these developments, valuable structural information can now be obtained in a relatively straightforward way for medium-sized biomolecules (see Vuister et al., 1998 and Griesinger et al, 1998 for reviews). Moreover, the newly measured J-coupling data have allowed the reparametrization of the Karplus curves describing the dependencies of the ^{3}J-values upon the intervening torsion angles (Vuister and Bax, 1993a, Wang and Bax, 1995, 1996; Hu and Bax, 1996; Hu and Bax, 1997b). It is to be expected that the newly obtained curves will be of higher accuracy compared to those derived solely on the basis of small model compounds, in particular for the range of dihedral angles which were actually used in the parametrization.

These new techniques can be subdivided on the basis of the underlying principle for measuring the J-coupling. In-phase-anti-phase (IPAP) methods are well-suited for the measurement of large- and rather uniform J-couplings (discussed in section 2). In the so-called E.COSY methods (Griesinger et al., 1985,1986,1987) (discussed in section 3) two spins are correlated without disturbing the energy levels of a third spin, which is J-coupled to both other spins. The resulting E.COSY pattern then allows the measurement of a small J-coupling, provided that the second J-coupling is large enough to allow separation of the multiplet components. E.COSY methods have now been used to measure a large variety of ^{2}J and ^{3}J-coupling constants (Montelione et al., 1989, Wider et al., 1989; Sörensen, 1990; Delaglio et al., 1991; Gemmecker and Fesik, 1991; Schmieder et al., 1991; Seip et al., 1992; Vuister and Bax, 1992; Emerson and Montelione, 1992; Eggenberger

et al., 1992; Griesinger and Eggenberger, 1992; Madsen et al., 1993; Weisemann et al., 1994a; Wang and Bax, 1995, 1996; Löhr and Rüterjans, 1995, 1997, 1999; Löhr et al., 1997).

A second class of experiments (discussed in section 4) aims to quantify the signal modulation or attenuation resulting from the active coupling and is referred to as quantitative J-correlation experiments (QJ) (Archer et al., 1991; Grzesiek et al., 1992; Blake et al., 1992; Billeter et al., 1992; Vuister and Bax, 1993a,b; Vuister et al., 1993a,b; Bax et al., 1994; Vuister et al., 1994; Kuboniwa et al., 1994; Grzesiek et al., 1995; Hu and Bax, 1996; 1997ab; Hu et al., 1997; Hennig et al., 1997).

Alternative methods for measuring J-couplings include the so-called P-FIDS or C'-FIDS methods (Schwalbe et al., 1994; Rexroth et al., 1995a) and the ZQ/DQ methods (Rexroth et al., 1995b; Otting, 1997).

1.1 Motivations for measuring J-couplings

There can be several reasons for measuring J-couplings:

- J-couplings can provide structural information
- Data can provide stereo-specific assignments.
- Data can provide dynamic information.
- Data can be used for structure validation.
- The same techniques are used for measurements of residual dipolar couplings and hydrogen-bond J couplings (^{h}J).

2. In-phase/antiphase methods (IPAP)

Methods to measure J-couplings from the superposition of in-phase and anti-phase (IPAP) are quite straightforward to implement and yield good success in cases of large- and uniform couplings (Sörensen et al., 1997). In particular, for measuring the effects of residual dipolar couplings on ^{1}J splittings, IPAP experiments are very useful. A schematic outline of the idea is shown in Figure 1. Simultaneous acquisition of either the sum or the difference of in-phase and anti-phase pattern yields one of the two multiplet components.

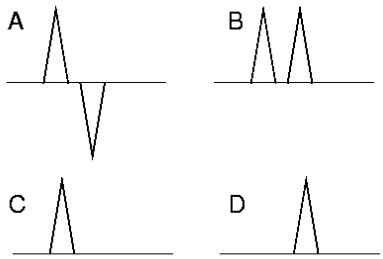

Figure 2.1. Schematic outline of anti-phase (A), in-phase (B) patterns, and sum (C) and difference (D) of these two patterns.

The concept can best be understood by evaluating the effect of the ^{15}N IPAP-HSQC sequence shown in Figure 2 as an example. In general, the transformation of an I_z operator under a β_ϕ pulse is given by:

$$I_z = I_\alpha - I_\beta \xrightarrow{\beta_\phi} I_z \cos\beta + I_x \sin\beta \sin\phi - I_y \sin\beta \cos\phi \qquad (2.1)$$

Hence, from time point a, we evaluate the effect of the $2H_zN_z$ operator :

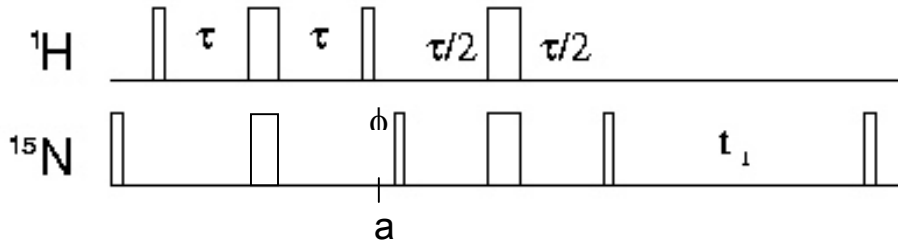

Figure 2.2. Schematic pulse scheme for an IPAP element.

$$2H_zN_z \xrightarrow{90^N_\phi} 2H_zN_x \sin\phi - 2H_zN_z \cos\phi \tag{2.2}$$

$$\xrightarrow{\pi J\tau} 2H_zN_x \sin\phi\cos(\pi J\tau) + N_y \sin\phi\sin(\pi J\tau)$$
$$-2H_zN_y \cos\phi\cos(\pi J\tau) + N_x \cos\phi\sin(\pi J\tau) \tag{2.3}$$

By setting :

$$\pi J\tau = \pi/4 \qquad \text{and} \qquad \phi = \pi/4 \quad or \quad 5\pi/4$$

we can select for the appropriate operator terms to get either the sum or differences of the in-phase and anti-phase patterns; i.e. both multiplet components in separate spectra by proper combination.

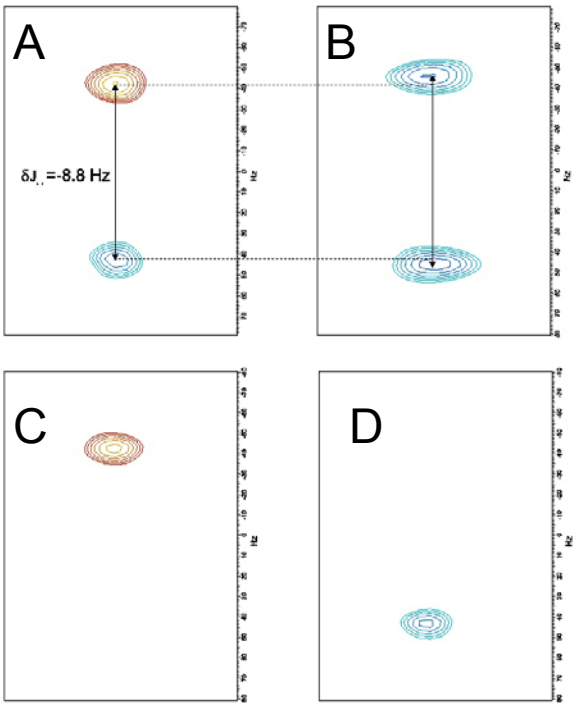

Figure 2.3 Small section of the ^{15}N-IPAP HSQC of ^{15}N-labelled EH2. Spectra A, C, and D were recorded in isotropic phase showing both component of the doublet (A), high-and low-field components (C,D). Spectrum D was recorded in aligned phase and shows an increased splitting due to residual dipolar couplings.

3. The E.COSY Methods.

The E.COSY (exclusive COSY) method was first proposed for homonuclear spin systems for the extraction of J-coupling constants and is formally equivalent to a superposition of multiple-quantum filtered spectra with appropriate weighting (Griesinger et al., 1985,1986,1987). For unlabeled proteins, yielding homonuclear 2D COSY-like spectra, the method has not gained widespread usage. However, the advent of ^{15}N and ^{13}C labeling in proteins has turned this method into a valuable tool for measuring J-couplings.

As proposed by Wang and Bax (1995), in the subsequent sections the different E.COSY schemes will be referred to by the experiment name from which they are derived, while the passive unperturbed spin will be indicated between square brackets. Thus, the HNCA E.COSY experiment (Smieder et al., 1991; Seip et al., 1992,1994; Madsen et al., 1993) for measuring $^{3}J(H^{N}H\alpha)$ (*vide infra*) will be denoted HNCA[Hα].

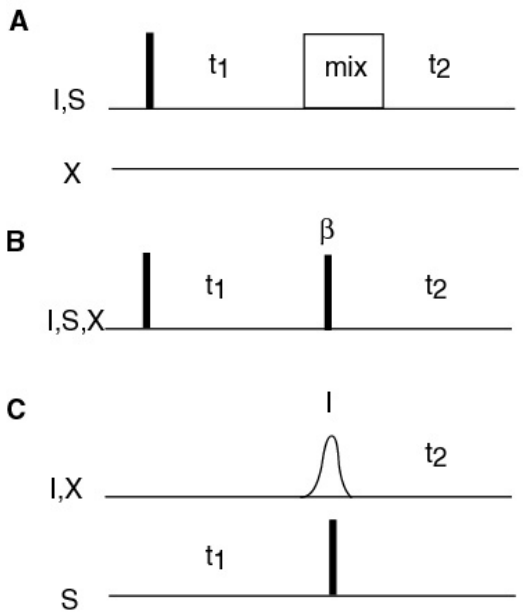

Figure 3.1.
Schematic outline of three E.COSY schemes. In scheme A, both the I- and S-spins are heteronuclear to spin X. In scheme B, all three spins I, S, and X are homonuclear. In scheme C, spins I and X are heteronuclear to spin S. Refer to text for further details.

3.1. Explanation of the E.COSY principle.

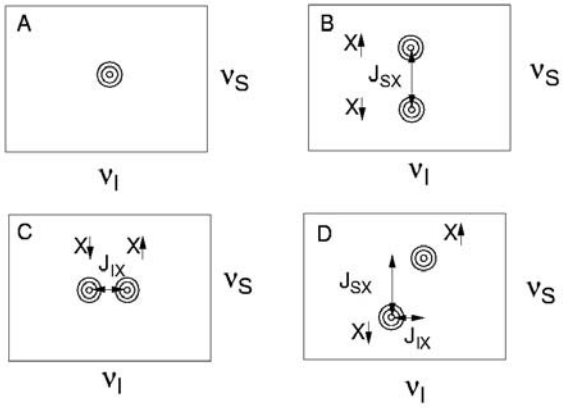

Figure 3.2. Schematic outline of the E.COSY principle. A) J(SX) interaction decoupled in t_1 and J(IX) interaction decoupled in t_2. B) J(SX) interaction active in t_1 and J(IX) interaction decoupled in t_2. C) J(SX) interaction decoupled in t_1 and J(IX) interaction active in t_2. D) J(SX) interaction active in t_1 and J(IX) interaction active in t_2, while assuming that the transfer of magnetization from S to I has not disrupted the spin state of X.

The E.COSY method allows the measurement of an (partially) unresolved coupling between spins I and X, J_{IX}, if there is a third spin S which has a large, resolved J-coupling with the X-spin, J_{SX}. In addition, it must be possible to transfer magnetization between the I- and S-spins without disturbing the spin state of the X-nucleus. The principle is most easily understood by considering two spins I and S, both heteronuclear to spin X (cf. Fig. 3.1A). The $(F_1,F_2) = (\nu_S,\nu_I)$ cross peak is shown in Fig. 3.2A in the absence of J-interactions with the X-nucleus in t_1 and t_2. Suppose the large J_{SX} interaction is now present during t_1. Consequently, the $(F_1,F_2) = (\nu_S,\nu_I)$ cross peak will show an in-phase doublet splitting along the F_1 axis resulting from this interaction (cf. Fig. 3.2B), the upfield component being associated with the X-spin in the α-state and the downfield shifted component being associated with the X-spin in the β state (assuming $J_{SX}>0$). Likewise, interaction between the I-spin and the X-spin during t_2 would result in a doublet splitting along the F_2 axis (cf. Fig. 3.2C), which may or may not be resolved. If however, the J-interactions J_{SX} and J_{IX} are active during t_1 and t_2, respectively, and the spin state of the X-nucleus is preserved during the transfer of magnetization between the I and S-spins the E.COSY pattern depicted in Fig. 3.2D will be generated since each of the two components of the multiplet is now displaced along both the F_1 and the F_2 axes.

An alternative explanation of the E.COSY pattern can be constructed in terms of the product operator formalism (Sörensen et al., 1983) by realising that the E.COSY pattern results from the superposition of an double in-phase multiplet with a double antiphase multiplet (cf. Fig. 3.3). Taking again the simple case of spins I and S, both heteronuclear to spin X, and evaluating the

effects of the pulse sequence depicted in Fig. 3.1A, the transverse S-magnetization, generated by the first 90û(I,S) pulse, evolves under the influence of chemical shift and J_{SX} interaction:

$$\begin{aligned} S_y \xrightarrow{t_1} & S_y \cos(\omega_S t_1)\cos(\pi J_{SX} t_1) - S_x \sin(\omega_S t_1)\cos(\pi J_{SX} t_1) \\ & - 2S_x X_z \cos(\omega_S t_1)\sin(\pi J_{SX} t_1) - 2S_y X_z \sin(\omega_S t_1)\sin(\pi J_{SX} t_1) \end{aligned} \quad (3.1)$$

The mixing period selects one of the quadrature components of the magnetization terms of eq. 3.1 and transfers magnetization from the S-spin to the I-spin without disturbing the X-spin polarization:

$$(3.1) \xrightarrow{mix} I_y \cos(\omega_S t_1)\cos(\pi J_{SX} t_1) - 2I_y X_z \sin(\omega_S t_1)\sin(\pi J_{SX} t_1) \quad (3.2)$$

$$\begin{aligned} (3.2) \xrightarrow{t_2} & \{I_y \cos(\omega_I t_2) - I_x \sin(\omega_I t_2)\} \cos(\pi J_{IX} t_2)\cos(\omega_S t_1)\cos(\pi J_{SX} t_1) \\ & - 2X_z \{I_x \cos(\omega_I t_2) + I_y \sin(\omega_I t_2)\} \sin(\pi J_{IX} t_2)\cos(\omega_S t_1)\cos(\pi J_{SX} t_1) \\ & - 2X_z \{I_y \cos(\omega_I t_2) - I_x \sin(\omega_I t_2)\} \cos(\pi J_{IX} t_2)\sin(\omega_S t_1)\sin(\pi J_{SX} t_1) \\ & + \{I_x \cos(\omega_I t_2) + I_y \sin(\omega_I t_2)\} \sin(\pi J_{IX} t_2)\sin(\omega_S t_1)\sin(\pi J_{SX} t_1) \end{aligned} \quad (3.3)$$

The I-spin now evolves during t_2 under the influence of of chemical shift and J_{IX} interaction:

$$\begin{aligned} (3.3) \xrightarrow{t_2} & \{I_y \cos(\omega_I t_2) - I_x \sin(\omega_I t_2)\} \cos(\pi J_{IX} t_2)\cos(\omega_S t_1)\cos(\pi J_{SX} t_1) \\ & - 2X_z \{I_x \cos(\omega_I t_2) + I_y \sin(\omega_I t_2)\} \sin(\pi J_{IX} t_2)\cos(\omega_S t_1)\cos(\pi J_{SX} t_1) \\ & - 2X_z \{I_y \cos(\omega_I t_2) - I_x \sin(\omega_I t_2)\} \cos(\pi J_{IX} t_2)\sin(\omega_S t_1)\sin(\pi J_{SX} t_1) \\ & + \{I_x \cos(\omega_I t_2) + I_y \sin(\omega_I t_2)\} \sin(\pi J_{IX} t_2)\sin(\omega_S t_1)\sin(\pi J_{SX} t_1) \end{aligned} \quad (3.4)$$

Realizing that

$$\begin{aligned} \cos(A)\cos(B) &= \tfrac{1}{2}\{\cos(A-B) + \cos(A+B)\} \\ \sin(A)\sin(B) &= \tfrac{1}{2}\{\cos(A-B) - \cos(A+B)\} \end{aligned} \quad (3.5)$$

and that only the first- and last terms of eq. 3.4 contain observable operators which result in the double in-phase pattern shown in Fig. 3.3A, and the double antiphase pattern shown in Fig. 3.3B, respectively. The superposition results in cancellation of half of the multiplet components (cf. Fig.

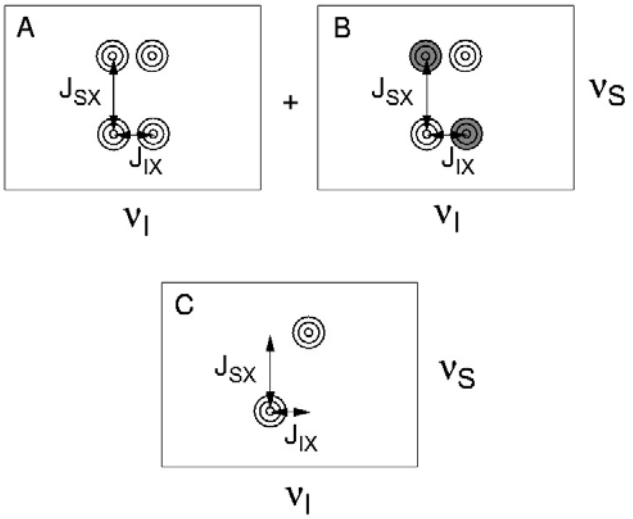

Figure 3.3.
Schematic multiplet patterns illustrating the E.COSY principle in terms of product operators. The superposition of a double in-phase pattern (A) with a double antiphase pattern (B) results in the E.COSY pattern (C) due to cancellation of half of the components (grey shaded cross peak components have a negative intensity).

3.3C), and the magnitude of the J_{IX} coupling can be determined from the displacement of the two multiplet components along the F_2 axis. Note that the presence of additional passive couplings to either spin I or spin S results in an additional in-phase splitting along the F_2 or F_1 axis, respectively.

The situation in which the X-spin is heteronuclear to both I- and S-spins presents the simplest case of the E.COSY experiment, in that the X-spin can be left unperturbed by simply applying no pulses to this nucleus. In case the X-spin is homonuclear to both the I- and S-spins, as is shown in Fig. 2B, the transition within the multiplet must be preserved by the application of a β-pulse. The use of a β flip angle in the so-called β-COSY (Bax and Freeman, 1981a,b), represents a compromise between proper cancellation of the different multiplet patterns on the one hand and sensitivity on the other hand. Alternatively, the β-pulse can be replaced by a multiple-quantum filter together with appropriate superposition as in the original E.COSY experiment (Griesinger et al., 1985,1986,1987).

A third situation encountered often, in particular in the case of $^{13}C/^{15}N$ labeled proteins, is shown in Fig. 2C. Here, the S-spin is heteronuclear to the I- and X-spins. In transfering the magnetization from I to S, the X-spin has to remain invariant. Hence, pulses applied in this transfer sequence must be selective for the I-spin. Non-selective sequences that effectively restore the original X-state, such as the sensitivity-enhancement scheme (Palmer et al., 1991; Kay et al., 1992), also fall in this category.

3.2 E.COSY ^{1}J and ^{2}J example

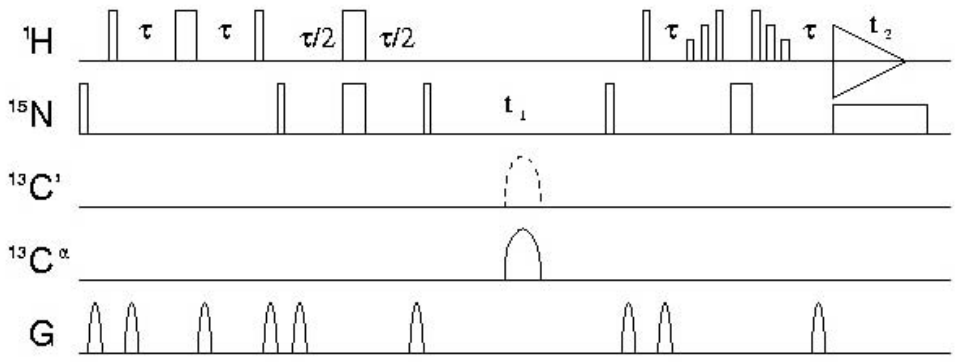

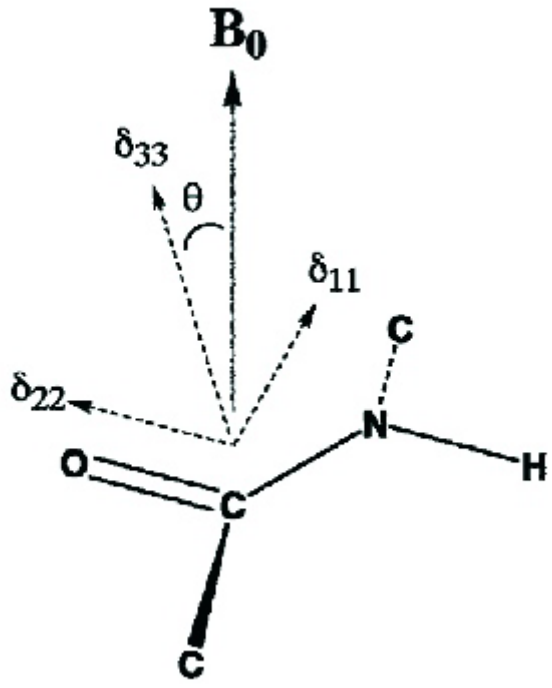

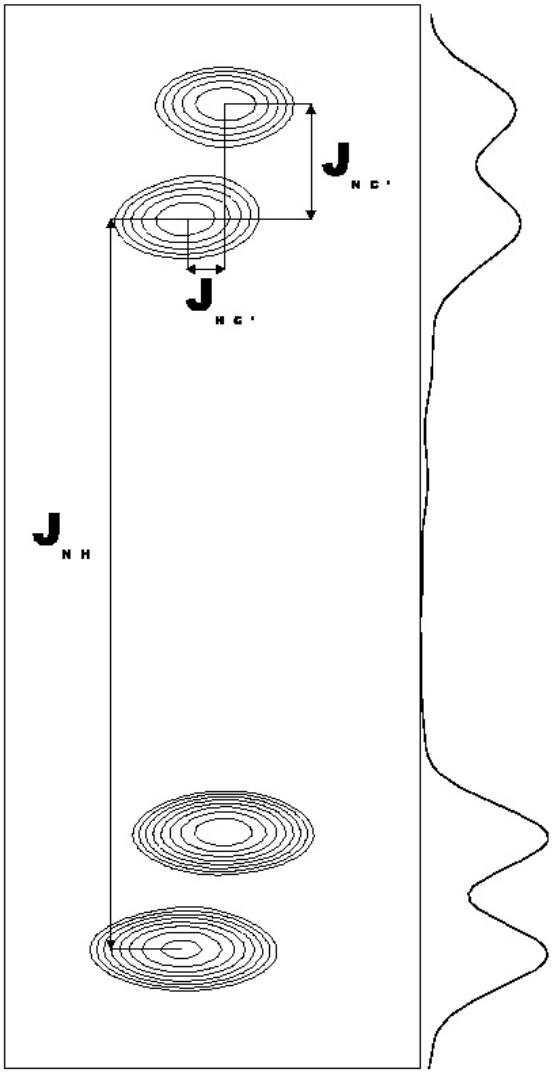

3.3 Practical outline E.COSY

1. Record the appropriate experiment.
2. Process assuring sufficient digital resolution (relative to J-coupling) in the dimension from which the J-coupling is to be measured.
3. Pick peaks using a peak-picker that does some form of interpolation. Pick only well-resolved peaks with sufficient signal-to-noise ratio.
4. Assure that peaks-files are written with sufficient precision (switch to Hz preferentially).
5. Extract J-couplings from the appropriate peaks.
6. When appropriate: analyze data again using deconvolution methods in time- and frequency domain.

4. The quantitative J-correlation Methods.

A suite of experimental techniques, commonly referred to as the quantitative J-correlation method (QJ), for measuring a diverse array of J-couplings has been developed in recent years (Archer et al., 1991; Grzesiek et al., 1992; Vuister and Bax, 1993a,b; Vuister et al., 1993a,b; Bax et al., 1992, 1994; Vuister et al., 1994; Grzesiek et al., 1995; Hu and Bax, 1996; 1997ab; Hu et al., 1997; Hennig et al., 1997). In the QJ method, the magnetization is allowed to dephase under the influence of a J-coupling for a constant period of duration T. The magnitude of the resulting in-phase and antiphase magnetization terms are determined, and the J-coupling can be extracted from the ratio of these terms.

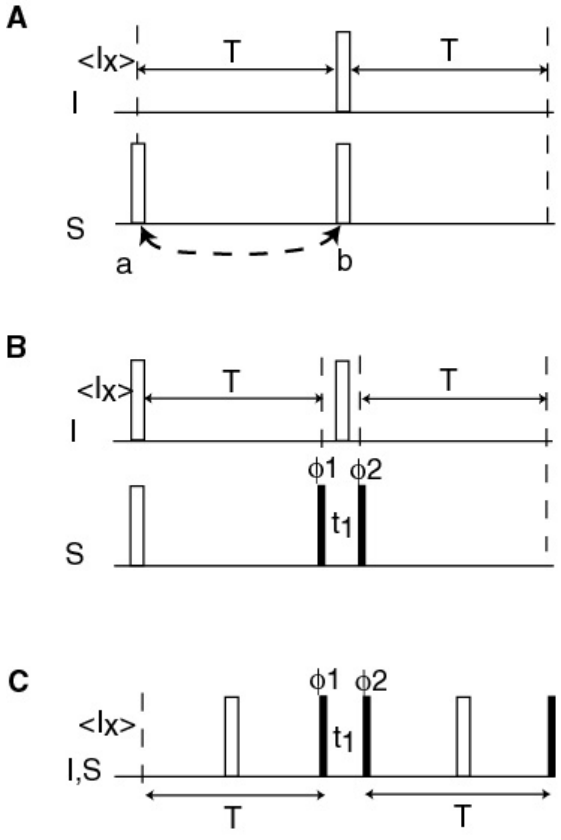

Figure 4.1.
Three schemes of the quantitative J-correlation method for determining J-couplings. Refer to the text for a full explanation. The phases in schemes B and C assume the presence of an I_x operator at the start of the pulse sequence element.
A) QJ-scheme based upon a spin-echo difference experiment. The 180° S-pulse is applied at position a *for the reference experiment and position* b *for the experiment in which the J-interaction is active.*
B) QJ-scheme based upon the HMQC experiment. The phases are ϕ_1 = x,-x; ϕ_2 = 2x,2(-x); receiver = x,2(-x),x or 4x (for the reference). The dashed 180°(I,S) pulses are optional and can be used for chemical shift labeling of the I-spin.
(C) QJ-scheme based upon the COSY experiment. The phases are ϕ_1 = x,-x; ϕ_2 = 2x,2(-x); receiver = 4x.

4.1. Spin-echo based quantitative J-correlation schemes.

Figure 6 depicts the three different variations in which the QJ method can be used to measure the J-interaction between two J-coupled spins, I and S. The first variation is a spin-echo difference based scheme (cf. Fig. 4.1A). This scheme can be used when there is one spin, S, heteronuclear to the I-spin with a J-coupling, J_{IS}. Assuming transverse magnetization of the I-spin, generated by some preparation sequence, the J_{IS} interaction is active for the full duration of 2T when the 180°(S) pulse is applied at position *b*:

$$I_x \xrightarrow{2T} I_x \cos(2\pi J_{IS} T) + 2 I_y S_z \sin(2\pi J_{IS} T) \tag{4.1}$$

where I and S denote the spin operators in the product operator formalism (Sörensen et al., 1983). Typically, the $2I_yS_Z$ term does not result in observable magnetization or can be purged away. Application of the 180°(S) pulse in position *a* effectively decouples the IS interaction and a reference experiment is obtained. The magnetization detected in the reference experiment experiences identical relaxation- and other losses, such as those resulting from passive couplings, as compared to the experiment with the 180°(S) applied at time *b*. Hence, the J-coupling can be calculated from the normalized relative difference of the two spectra in a straightforward fashion:

$$\frac{S_b}{S_a} = \frac{A\cos(2\pi J_{IS} T)}{A} = \cos(2\pi J_{IS} T) \tag{4.2}$$

where S_a and S_b denote the signal obtained with the 180°(S) pulse in positions *a* and *b*, respectively. The presence of more spins J-coupled to the I-spin can be accommodated for, provided that the magnitude of these J-interactions is of known, and constant magnitude (Grzesiek et al., 1993). Note that chemical shift labeling of the I-spin can be easily implemented by moving the 180° pulses in concert in a constant-time fashion.

4.2. HMQC-based quantitative J-correlation schemes.

The second variation of the QJ method is based upon the HMQC experiment and shown in Figure 4.1B. This variation is most useful when there are multiple spins S_i, heteronuclear to spin I, with varying magnitude of the J-couplings J_{ISi}. Considering first an isolated IS-spin pair and assuming transverse I-spin magnetization generated by some preparation sequence, the J_{IS} coupling is active for the duration of T:

$$I_x \overset{T}{\rightarrow} I_x \cos(\pi J_{IS} T) + 2 I_y S_z \sin(\pi J_{IS} T) \tag{4.3}$$

The subsequent 90°(S,ϕ_1) pulse selects for the $2I_YS_Z$ component and converts it into heteronuclear multiple quantum terms. Chemical shift labeling with the S-spin frequency is obtained during t_1 in a pseudo-single quantum manner:

$$2 I_y S_y \overset{90_x \quad t_1}{\rightarrow\rightarrow} -2 I_y S_y \cos(\omega_S t_1) + 2 I_y S_x \sin(\omega_S t_1) \tag{4.4}$$

where the $\sin(\pi J_{IS}T)$ term of eq. 4.3 has been temporarily omitted from eq. 4.4. The subsequent 90°(S,ϕ_2) pulse selects one of the quadrature components and converts this back into antiphase magnetization which is allowed to rephase for a period T:

$$-2 I_y S_y \overset{90_x^S \quad T}{\rightarrow\rightarrow} -2 I_y S_Z \cos(\omega_S t_1)\cos(\pi J_{IS} T) + I_x \cos(\omega_S t_1)\sin(\pi J_{IS} T) \tag{4.5}$$

Only the I_X operator results in observable magnetization, so that after Fourier transformation with respect to t_1, the volume of the cross peak at the $F_1=\omega_S$ frequency, V_S, can be written as:

$$V_S = -A \sin^2(\pi J_{IS} T) \tag{4.6}$$

where the previously omitted trigonometric term has been reintroduced and *A* denotes a proportionality constant which incorporates all experimental factors, constant losses due to relaxation and other passive couplings, and the effects of data processing. A reference experiment,

selecting for the I_X operator of eq. 4.3, is obtained by changing the receiver phase cycle (cf. caption Fig. 4.1B). Obviously, the I_X operator does not evolve in t_1 and thus the dimensionality of the reference experiment is one lower, as compared to the first experiment. During the second period of duration T, the J_{IS}-coupling is again active:

$$I_x \cos(\pi J_{IS} T) \xrightarrow{T} I_x \cos^2(\pi J_{IS} T) + 2 I_y S_z \cos(\pi J_{IS} T) \sin(\pi J_{IS} T) \qquad (4.7)$$

Only the I_X term results in observable magnetization so that the volume of the reference peak, V_I, becomes:

$$V_I = -A' \cos^2(\pi J_{IS} T) \qquad (4.8)$$

where *A*' is a constant closely related to *A*. Assuming for simplicity momentarily identical transverse relaxation times of the in-phase and antiphase magnetization, the constants *A'* and *A* are related by a simple scaling factor resulting from the different Fourier transformations of both experiments (Vuister et al., 1993b). Thus, after scaling the magnitude of the J-coupling, J_{IS} can be easily calculated from the ratio of the cross-peak volumes:

$$\frac{V_S}{V_I} = -\tan^2(\pi J_{IS} T) \qquad (4.9)$$

In case of several spins S_i, it is straightforward to show that the additional spins act as passive spins in both versions of the experiment. The development of a small amount of double antiphase magnetization involving spins S_i and S_j, $4I_X S_i S_j$, potentially may result in small errors. However, because of the $\sin(\pi J_{ISi} T)\sin(\pi J_{ISj} T)$ dependence of this term it can safely be neglected (Vuister et al., 1993b). Hence, the expressions for the cross-peak volumes for the i^{th} S-spin, V_{Si}, and the reference, V_I, become:

$$V_{Si} = -A \sin^2(\pi J_{ISi} T) \prod_{j \neq i} \cos^2(\pi J_{ISj} T) \qquad (4.10a)$$

$$V_I = -A'\cos^2(\pi J_{ISi}T)\prod_{j\neq i}\cos^2(\pi J_{ISj}T) \tag{4.10b}$$

where J_{ISi} denotes the J-coupling between the I-spin and the i^{th} S-spin. From eq. 4.10 it can be seen that the terms involving spins S_j cancel when computing the ratio of V_{Si} and V_I:

$$\frac{V_{Si}}{V_I} = -\tan^2(\pi J_{IS}T) \tag{4.11}$$

which is identical to eq. 4.9. Chemical shift labeling of the I-spin can be implemented in a straightforward fashion, by shifting the dashed 180°(I,S) pulses in a constant-time manner.

4.3. COSY-based quantitative J-correlation schemes.

The third variation of the QJ method is shown in Figure 4.1C and based upon a COSY-type experiment. It can be used in the case of one or more spins S_i, homonuclear to spin I, with varying J-couplings, J_{ISi}. The scheme is highly analogous to the scheme discussed for the second variation of the QJ method (cf. Fig. 4.1B), albeit that reference- and cross peaks are present in one spectrum, thereby facilitating the analysis. Again, considering first only an isolated IS-spin pair and starting with transverse I-spin magnetization, the J_{IS} coupling is active for a duration T:

$$I_x \overset{T}{\rightarrow} I_x\cos(\pi J_{IS}T) + 2I_yS_z\sin(\pi J_{IS}T) \tag{4.12}$$

The 90°(ϕ_1) pulse now results in a COSY-like transfer:

$$\overset{90_x}{\rightarrow} I_x\cos(\pi J_{IS}T) - 2I_zS_y\sin(\pi J_{IS}T) \tag{4.13}$$

During the t_1 period, the maximum duration of which is short relative to $(J_{IS})^{-1}$, the I_X and $2I_ZS_Y$ operators precess with the ω_I and ω_S frequencies, respectively, resulting in:

$$\overset{t_1}{\rightarrow} I_x\cos(\omega_I t_1) + I_y\sin(\omega_I t_1) - 2I_zS_y\cos(\omega_I t_1) + 2I_zS_x\sin(\omega_I t_1) \tag{4.13}$$

where the earlier trigonometric terms have been dropped from eq. 4.14. The 90°(ϕ_2) pulse selects one of the quadrature components and converts the antiphase S-magnetization back to antiphase I-magnetization. During the rephasing period of duration T, the J_{IS} interaction is again active resulting in a total of four terms:

$$\overset{90^\circ}{\rightarrow}\overset{T}{\rightarrow}\{I_x\cos^2(\pi J_{IS}T)+2I_yS_z\cos(\pi J_{IS}T)\sin(\pi J_{IS}T)\}\cos(\omega_I t_1)+$$
$$\{2I_yS_z\cos(\pi J_{IS}T)\sin(\pi J_{IS}T)-I_x\sin^2(\pi J_{IS}T)\}\cos(\omega_S t_1) \quad (4.14)$$

The last 90° purge pulse again converts the antiphase terms, and thus only the I_X terms contribute to the observed I-spin signal.

$$\overset{90^\circ}{\rightarrow} I_x\{\cos^2(\pi J_{IS}T)\cos(\omega_I t_1)-\sin^2(\pi J_{IS}T)\cos(\omega_S t_1)\} \quad (4.15)$$

After Fourier transformation with respect to the t_1 dimension, peaks at the ω_I and ω_S frequencies are obtained along this frequency axis, referred to as the 'diagonal' and 'cross-peak', respectively. Reintroducing the earlier omitted trigonometric terms and neglecting differential relaxation of in-phase and antiphase terms momentarily, the volumes of the cross-peak, V_S, and diagonal peak, V_I, are written as:

$$V_S = -A\sin^2(\pi J_{IS}T) \quad (4.16a)$$
$$V_I = A\cos^2(\pi J_{IS}T) \quad (4.16b)$$

where A again denotes a proportionality constant that includes all experimental- and other constant factors. As above for the HMQC-based QJ methods, the magnitude of the J_{IS} coupling can be extracted in a straightforward fashion from the cross-peak to diagonal-peak ratio:

$$\frac{V_S}{V_I} = -\tan^2(\pi J_{IS} T) \tag{4.17}$$

In this experiment, similar to the second variation of the QJ method, the presence of several spins S_i which are J-coupled to spin I, results in additional passive coupling terms which cancel from the ratio V_{Si} / V_I. The J_{ISi} can therefore still be extracted from the cross-peak to diagonal-peak ratio using eq. 4.17.

As the maximum duration of the t_1 period typically is kept short compared to the transverse relaxation time of the I- and S-spins, the lineshape in the F_1 dimension is determined primarily by the apodization function. Consequently, the ratio of cross-peak intensity to diagonal-peak intensity yields almost identical results.

4.4 Practical outline QJ

1. Record the appropriate experiment assuring appropriate sampling in each dimension. Be aware that for some experiments long acquisition times in some of the indirect dimension will compromise the experiment.
2. Process assuring appropriate filtering and digital resolution each dimension.
3. Pick peaks (both 'diagonal' and 'cross-peak') using a peak-picker that does some form of interpolation. Pick also diagonal peaks for which no cross-peaks is observed. In these instances, the noise level of the experiment will provide an upper limit.
4. Assure that the intensity (volume) columns of the peaks-file is written with sufficient precision, and in absolute scaling mode.
5. Extract J-couplings using the appropriate peaks and formula. Be aware of the factor 'two' related to the dephasing period in these equations. Check your experiment to assure your definition matches. Correct for differential relaxation effect by applying a simple uniform correction factor (see Vuister and Bax, 1993 for the recipe). Use the noise level as cross-peak intensity to obtained upper-limit estimates in case no cross-peaks are observed.
6. When appropriate: analyze data again using deconvolution methods in time- and frequency domain; typically to extract more diagonal peaks.

5. Comparing the merits of E.COSY and QJ-methods

The two most commonly used schemes, E.COSY- and QJ-methods, both have specific advantages and disadvantages. E.COSY methods are suited equally well for the extraction of small- and large couplings, in addition to providing information about the relative signs of the coupling constants. The accuracy of its results are dependent upon the signal-to-noise ratio and the lineshape of the multiplet, and the extend to which the spin state of the passive nucleus can be preserved. Sometimes the spin-topology prohibits the E.COSY measurement and also overlap of different multiplets can present a problem. Moreover, the actual accurate determination of the coupling is somewhat more cumbersome when compared to the QJ-methods.

The extraction of the ^{3}J-values is simple for the QJ-based methods. In addition, in those cases were the spin-topology prohibits the E.COSY measurement, the QJ-methods sometimes can yield the ^{3}J-values. The lower limit of the coupling constants that can be determined by the QJ-based methods is set by the signal-to-noise ratio of the experiment, i.e. the size of the ^{3}J-value relative to the effective transverse relaxation time. If the relaxation is too fast relative to the magnitude of the J-coupling, a correlation is not observed and only an upper estimate of the J-value can be obtained. In addition, no information about the sign of the ^{3}J-value can be derived from the QJ-experiments.

Table 5.1. Comparison of the merits of E.COSY and QJ methods.

E.COSY	QJ
Equally well suited for large and small coupling constants	Lower limit determined by signal-to-noise (i.e. detectable cross peak)
Relative sign of the J-value	Only absolute sign of the J-value
Accuracy dependent upon signal-to-noise, lineshape, and preservation of the passive spin state	Accuracy determined by the differential relaxation of in-phase and anti-phase
Not all spin topologies can be tackled	Different spin-topologies possible
Resolution sometimes a problem (overlap of multiplets)	Resolution sometimes a problem (e.g. reference experiment)
Proper analysis requires time and effort	Analysis is simple

6. The backbone angle ϕ

Knowledge about the backbone angles ϕ and ψ is of great importance in restricting the conformational space of the backbone and thereby helps to establish the global fold of the protein. Historically, the $^3J(H^NH\alpha)$ has received most attention since it can be measured in a relatively straightforward way in small proteins, Therefore, information about the ϕ angle has been used in NMR structure determination as early as 1984 (Pardi et al., 1984).

6.1. J-Couplings related to ϕ.

Figure 6.1 shows the Fisher projection of a peptide fragment around the backbone angle ϕ. From the figure, it is evident that the torsion angle ϕ is associated with up to six ^3J-coupling constants. For non-glycine residues, these coupling constants are $^3J(H^NH\alpha)$, $^3J(H^NC\beta)$, $^3J(H^NC')$, $^3J(C'^{i-1}H\alpha)$, $^3J(C'^{i-1}C\beta)$, and $^3J(C^{i-1}C')$. Table 6.1 lists the experiments aimed at measuring these six coupling constants.

Since the magnitude of the $^3J(H^NH\alpha)$ is also relatively easy to determine in smaller polypeptides, a parametrization of the Karplus curve based upon protein data has been available for some time (Pardi et al., 1984). A recent reparametrization on the basis of a larger number of observations obtained from newer experiments (Vuister and Bax, 1993a; Wang and Bax, 1996) have adjusted the magnitude of the A, B, and C parameters somewhat, but have not changed the overall shape of the Karplus curve for $^3J(H^NH\alpha)$. The curves corresponding to three different parametrizations are shown in Figure 6.2A. The most recent one was obtained by Wang and Bax (1996) for ubiquitin using optimized dihedral angles (cf. curve with small dashes in Fig. 6.2A). Thus, all curves show that the $^3J(H^NH\alpha)$ value is approximately 10 Hz for β-sheet regions and in the range of 4-6 Hz for residues in α-helical conformation.

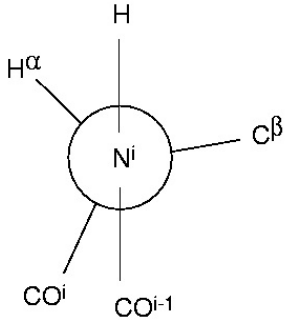

Figure 9. Fisher projection around the backbone torsion angle ϕ.

A second coupling constant related to the backbone angle ϕ is the $^3J(H^NC')$. It can be measured from the HNCA[C'] E.COSY experiment (Weisemann et al., 1994a; Seip et al., 1994; Wang and

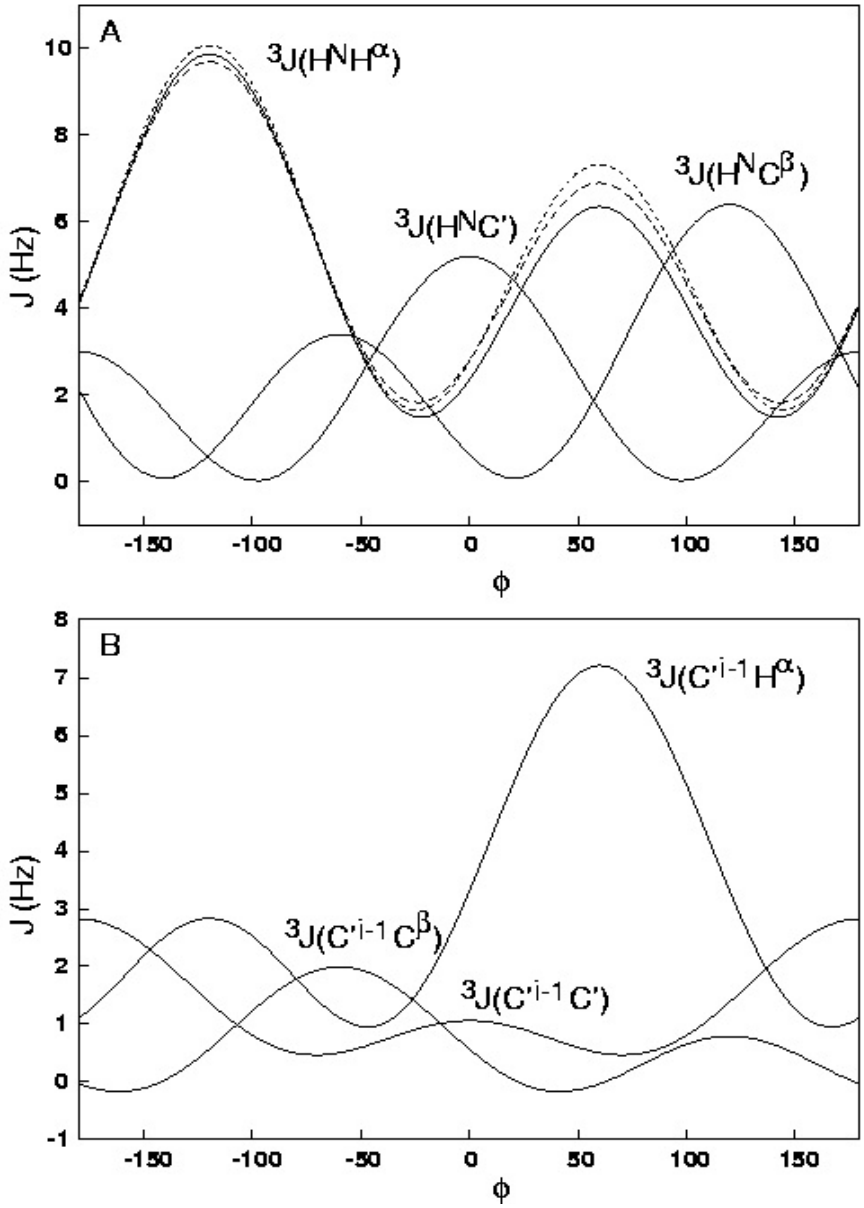

Figure 6.2. Karplus curves showing the dependencies of the (A) $^3J(H^NH\alpha)$, $^3J(H^NC')$, and $^3J(H^NC\beta)$ and (B) $^3J(C'^{i-1}H\alpha)$, $^3J(C'^{i-1}C\beta)$, and $^3J(C'^{i-1}C')$ coupling constants upon the torsion angle ϕ. Curves shown are: $^3J(H^NH\alpha) = A\ cos^2(\phi-60°) + B\ cos(\phi-60°) + C$ with A,B,C = 6.51,-1.76,1.60 (solid) (Vuister and Bax, 1993a); A,B,C = 6.41,-1.46,1.9 (large dashes) (Pardi et al., 1984), and A,B,C = 6.98,-1.38,1.72 (small dashes) (Wang and Bax, 1996). $^3J(H^NC') = 4.0\ cos^2(\phi\pm180°) - 1.1\ cos(\phi\pm180°) + 0.1$ (Wang and Bax, 1995, 1996). $^3J(H^NC\beta) = 4.7\ cos^2(\phi+60°) - 1.5\ cos(\phi+60°) + 0.2$ (Bystrov, 1976). $^3J(C'^{i-1}H\alpha) = 3.75\ cos^2(\phi+120°) - 2.19\ cos(\phi+120°) + 1.28$ (Wang and Bax, 1996). $^3J(C'^{i-1}C\beta) = 1.5\ cos^2(\phi-120°) - 0.6\ cos(\phi-120°) - 0.1$ (Bystrov, 1976). $^3J(C'^{i-1}C') = 1.33\ cos^2(\phi) - 0.88\ cos(\phi) + 0.62$ (Hu and Bax, 1996). NB. Unfortunately, Wang and Bax (1995,1996) incorporate a 180° phase shift into their equations for $^3J(H^NC')$ and $^3J(C'^{i-1}H\alpha)$ by defining the dihedral angle ϕ as $H^{Ni}\text{-}N^i\text{-}C^{\alpha i}\text{-}C'$ instead of the IUPAC definition $C'^{i-1}\text{-}N^i\text{-}C^{\alpha i}\text{-}C'^i$ (IUPAC, 1970).

.Bax, 1995). Values of this coupling constant recently determined for ubiquitin prompted also for a reparametrization of the Karplus curve which substantially differs from the parametrization obtained from the studies on small model compounds (Wang and Bax, 1995). The resulting curve is also shown in Fig. 6.2A, and illustrates the complementarity to the $^3J(H^NH\alpha)$, but also the rather limited range of the $^3J(H^NC')$ coupling constant in proteins

A third coupling constant yielding information about the backbone angle ϕ is the $^3J(H^NC\beta)$. This coupling constant has been measured in an E.COSY fashion from 3D ^{15}N-separated NOESY[C] or 4D $^{13}C/^{15}N$-separated NOESY[C] experiments on a fully $^{13}C/^{15}N$ labeled protein (Seip et al., 1994) or by using an HNCA-based E.COSY experiment employing selective Cα pulses (Löhr and Rüterjans, 1995; Wang and Bax, 1996). Reparametrization of the corresponding Karplus relationship on the basis of the values measured for ubiquitin (Wang and Bax, 1996) again substantially changed the earlier curve derived on the basis of FPT-INDO calculations, most notably in the region of positive ϕ values. However, as only two experimental datapoints were obtained with $^3J(H^NC\beta)$ values corresponding to $\phi>0$, the maximum of the $^3J(H^NC\beta)$ Karplus curve (at $\phi=120°$) may be ill-determined. In fact, reparametrization using refined backbone angles substantially changed this maximum. Unfortunately, the range of $^3J(H^NC\beta)$ values in proteins will be rather limited since the maximum value is found for ϕ-angles which are conformationally disallowed in proteins. Therefore, the applicability will critically depend on the accuracy of the measurement of the $^3J(H^NC\beta)$ values.

The fourth coupling constant related to ϕ is the $^3J(C'^{i-1}C')$. This coupling constant can be measured from the HN(CO)CO experiment (Hu and Bax, 1996) in a straightforward fashion. Recent reparametrization of the Karplus curve for $^3J(C'^{i-1}C')$ was also performed using the values obtained for ubiquitin (Hu and Bax, 1996). The result is shown in Figure 6.2B and indicates that this coupling constant is predominantly useful in restricting the backbone angle ϕ for values around $\pm180°$. For β-sheet regions, however, it can provide useful additional information as the $^3J(H^NH\alpha)$ curve allows for two possibilities when the measured $^3J(H^NH\alpha)$ values are in the 8-9 Hz range. The steep dependence of $^3J(C'C')$ on ϕ then allows for a discrimination between these two possibilities.

Values for the $^3J(C'^{i-1}H\alpha)$ coupling constant have recently also been measured in proteins (Löhr and Rüterjans, 1995,1997; Wang and Bax, 1996) and its Karplus-type dependence on the torsion angle ϕ has recently be reparametrized using the values measured in ubiquitin (Wang and

Bax, 1996). The corresponding curve is shown in Fig 6.2B and shows that a substantial larger value is expected for ϕ=60° as compared to the range of negative values of ϕ. Hence, it is a useful coupling constant for identification of residues in the positive region of the Ramanchandran plot.

The $^{3}J(C'^{i-1}C\beta)$ is the last coupling constant for which values measured in proteins have become available and its Karplus-type dependence on the torsion angle ϕ has recently also be reparametrized (Hu and Bax, 1997b).

Table 6.1. Experiments for Measuring *J* Couplings Related to ϕ.

Coupling	Experiment[a]	Reference	Labeling	Remark
$^3J(H^NN^\alpha)$	COSY	Pardi *et al.* (1984)	-	From splittings in COSY
	COSY/NOESY	Ludvigsen *et al.* (1991)	-	DISCO-like procedure
	^{15}N HMQC	Kay *et al.* (1989) Kay and Bax (1990)	^{15}N	High-resolution HMQC
	HNCA[H^α]	Schmieder *et al.* (1991)	$^{15}N/^{13}C$	Different schemes for leaving H^α untouched
		Seip *et al.* (1994)		
		Madsen *et al.* (1993)		
		Görlach *et al.* (1993)		15N-$^1H^N$ MQ scheme
		Weisemann *et al.* 1994a)		
		Tessari *et al.* (1995)		
		Löhr and Rüterjans (1995)		
		Wang and Bax (1996)		Selective H^N pulses in revINEPT
	(H)NCAHA[H^N]	Löhr and Rüterjans (1995)	$^{15}N/^{13}C$	H^α detection in H_2O
	HSQC/HMQC-J	Neri *et al.* (1990) Billeter *et al.* (1992)	^{15}N	
		Kuboniwa *et al.* (1994)		CT version
	HNHA	Vuister and Bax (1993a)	^{15}N	
		Kuboniwa *et al.* (1994)		
	CT-HMQC-HA/HN	Ponstingl & Otting (1998)	^{15}N	
	S^3E-sequences	Sorensen *et al.*, (1997)	^{15}N	Selective exitation of one of the multiplet components
$^3J(H^NC')$	HNCA[C′]	Weisemann *et al.* (1994a) Seip *et al.* (1994) Wang and Bax (1995)	$^{15}N/^{13}C$	
	(H)CANNH[C′]	Löhr and Rüterjans (1995)	$^{15}N/^{13}C$	
$^3J(H^NC^\exists)$	3D/4D-separated NOESY[$C^\exists$]	Seip *et al.* (1994)	$^{15}N/^{13}C$	
	(H)CANNH[$C^\exists$]	Löhr and Rüterjans (1995)	$^{15}N/^{13}C$	Requires C^α selective pulses
	HNCA[C∃]	Wang and Bax (1996)	$^{15}N/^{13}C$	Requires C^α selective pulses
	HNCACB[H^N]	Löhr and Rüterjans (1999)	$^{15}N/^{13}C$	
$^3J(C'^{i-1}H^\alpha)$	(H)NCAHA[C′]	Löhr and Rüterjans (1995)	$^{15}N/^{13}C$	
	HCAN[C′]	Wang and Bax (1996)	$^{15}N/^{13}C$	Sample in D_2O preferable
	H(N)CA,CO[H^α]	Löhr and Rüterjans (1997)	$^{15}N/^{13}C$	
	HN(CO)HB	Grzesiek *et al.* (1992)	$^{15}N/^{13}C$	Separate reference experiment
	H(N)CA,CO[C^α]	Löhr *et al.*, 1997	$^{15}N/^{13}C$	
$^3J(C'^{i-1}C')$	HN(CO)CO	Hu and Bax (1996)	$^{15}N/^{13}C$	
	H(N)CA,CO[CO]	Löhr *et al.*, 1997	$^{15}N/^{13}C$	
$^3J(C'^{i-1}C^\exists)$	HN(CO)C	Hu and Bax (1997b)	$^{15}N/^{13}C$	
	H(N)CA,CO[C^β]	Löhr *et al.*, 1997	$^{15}N/^{13}C$	
	HNCACB[CO]	Löhr and Rüterjans (1999)	$^{15}N/^{13}C$	

[a]Experiments are named analogous to the nomenclature proposed for triple-resonance experiments (Ikura *et al.* 1990). The passive spin in the E.COSY-type experiment is indicated in square brackets (Wang and Bax, 1995).

7. The backbone angle ψ

The backbone torsion angle ψ is far less amenable to analysis using J-couplings (cf. Table 7.1). The Fisher projection is shown in Figure 7.1. In fact, as the $^3J(N^iN^{i+1})$ coupling constants are of vanishing small magnitude (Bystrov, 1976; Theis et al., 1997), only the $^3J(H^{\alpha i}N^{i+1})$ and $^3J(C^{\beta i}N^{i+1})$ coupling constants potentially provide information about the torsion angle ψ. E.COSY-type measurements employing either the H^α as the passive spin (Weisemann et al., 1994a; Seip et al., 1994) or the nitrogen as a passive spin (Wang and Bax, 1995) have been used for measuring $^3J(H^{\alpha i}N^{i+1})$. Alternatively, the HSQC-NOESY[N] (Wider et al., 1989) or HNHB experiment (Archer et al., 1991; Madsen et al., 1993; Düx et al., 1997a) provides the correlation to the sequential H^α from which the $^3J(H^{\alpha i}N^{i+1})$ can be derived. Although in the latter experiment the ^3J-couplings to the H^β act as passive couplings that attenuate the sequential H^α correlation, for residues with $-150° < \psi < 0°$ it is quite feasible to measure $^3J(H^{\alpha i}N^{i+1})$ in well-behaved proteins.

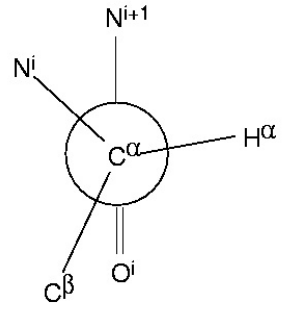

Figure 7.1. Fisher projection of the backbone torsion angle ψ.

Recently measured values of $^3J(H^{\alpha i}N^{i+1})$ coupling constants in ubiquitin using the HCACO[N] E.COSY experiment have been used to reparametrize the Karplus curve describing the dependence of the $^3J(H^{\alpha i}N^{i+1})$ on ψ (Wang and Bax, 1995). The resulting curve is shown in Figure 7.2. Also shown in this figure are the experimental $^3J(H^{\alpha i}N^{i+1})$ values measured for PYP using a modified HNHB experiment (Düx et al., 1997a). The experimental ^3J-values match the shape of the curve reasonably well, exhibiting the largest (negative) values around $\psi \sim -60°$. However, the data also suggest a somewhat lower minimum, in agreement with results obtained before for Ribonuclease T1 (Karimi-Nejad, 1996). Substituent effects (Haasnoot et al., 1980) could also be responsible for this effect as these have been deemed (partially) responsible for the scatter observed between theoretical- and experimental values (Wang and Bax, 1995).

The detection limit of the correlations to the sequential H^α determines the lower limit of the $^3J(H^{\alpha i}N^{i+1})$ couplings that can be obtained from the HNHB experiment. Thus, for PYP correlations corresponding to coupling constants < 0.7 Hz were not observed, i. e. no data were obtained for ψ >

0° or ψ < -150°. In principle, the E.COSY HSQC-NOESY[N] experiment will allow for the measurement of smaller couplings, albeit that the accuracy of the method depends upon the intensity of the sequential $H^{\alpha i}$-H^{Ni+1} cross peak.

Regarding the small ^{3}J(C'N) values measured in proteins so far (Vuister et al., 1993a; Hu et al., 1997; Hu and Bax, 1997a), the $^3J(C'^iN^{i+1})$ values across the peptide bond are expected to be small and no experimental data have thus far been reported for proteins.

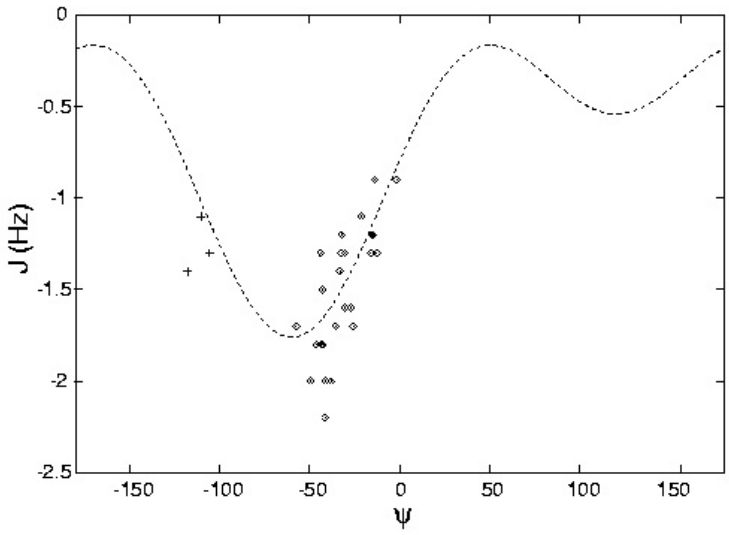

Figure 7.2.
Experimental $^3J(H^{\alpha i}N^{i+1})$ values of PYP measured using the modified HNHB experiment (Düx et al., 1996a) versus *ψ-values of the refined average structure (Düx et al., 1997b). Glycine $^3J(H^{\alpha 3}N^{i+1})$ values are indicated by '+' and are offset in ψ by –120°. Karplus curve describing the dependence of the $^3J(H^{\alpha i}N^{i+1})$ on ψ, using parameters were taken from Wang and Bax (1995): $^3J(H^{\alpha i}N^{i+1}) = -0.88\ cos^2(\psi-120°) - 0.61\ cos(\psi-120°) - 0.27$. Note that in the original parameterization the authors used a 180° phase shift in their definition of the dihedral angle ψ with respect to the IUPAC definition (IUPAC, 1970), which has been used here.*

Table 7.1. Experiments for Measuring *J* Couplings Related to *ψ*.

Coupling	Experiment[a]	References	Labeling	Remark
$^3J(H^{\alpha}N^{i+1})$	NOESY[N]	Montelione *et al.* (1989)	^{15}N	E.COSY on $d_{\alpha N}$
	HSQC-NOESY[N]	Wider *et al.* (1989)	^{15}N	E.COSY on $d_{\alpha N}$
	HNHB	Archer *et al.* (1991) Madsen *et al.* (1993) Düx *et al.* (1997)	^{15}N	
	HN(CO)CA[H^{α}]	Seip *et al.* (1994)	^{15}N/^{13}C	
	HCACO[N]	Wang and Bax (1996)	^{15}N/^{13}C	Sample in D_2O
^3J(NN)		Theis *et al.* (1997)	^{15}N	

[a]Experiments are named analogous to the nomenclature proposed for triple-resonance experiments (Ikura *et al.* 1990). The passive spin in the E.COSY-type experiment is indicated in square brackets (Wang and Bax, 1995).

8. The sidechain angles χ_1 and χ_2

Information of the χ_1 rotameric state and stereospecific assignment of β-methylene protons is of great importance to the structure determination process. Figure 8.1 shows the Fisher projection around the sidechain angle χ_1, which illustrates that, for the majority of amino acids, this information can be obtained from as many as nine different ^{3}J-coupling constants. In practice however, not all of these can be measured straightforwardly and a summary of the experiments aimed at measuring a selection of these ^{3}J coupling constants is presented in Table 3. The Karplus curves describing the dependencies of $^3J(H^\alpha H^{\beta 2})$, $^3J(H^\alpha H^{\beta 3})$, $^3J(H^\alpha C^\gamma)$, $^3J(C'H^{\beta 2})$, $^3J(C'H^{\beta 3})$, $^3J(NH^{\beta 2})$, and $^3J(NH^{\beta 3})$ upon the torsion angle χ_1 are shown in Figure 7.2.

Parametrization of all these curves is based upon studies on small model compounds and/or *ab initio* calculations, as no parametrizations using protein data are available. For example, two curves for $^3J(H^\alpha H^{\beta 2})$ are shown (DeMarco et al., 1978a; Bystrov, 1976) which differ by almost 2 Hz in their maximum value observed for $\chi_1 = -60°$. In analogy to the large changes in the ϕ-dependent Karplus curves, observed upon re-parametrizations using protein data (cf. section 6), it can be expected that the χ_1-dependent Karplus curves will also substantially change once accurate protein data become available.

For some ^{3}J-coupling constants, such as $^3J(NC^\gamma)$ or $^3J(C'C^\gamma)$, no parametrizations are available. Values measured in proteins, however, suggest narrow ranges for these two coupling

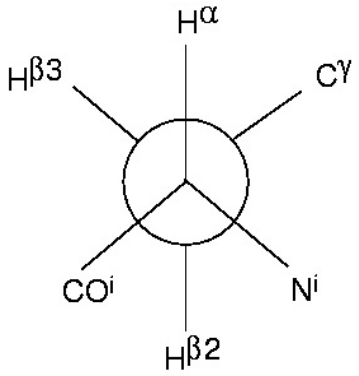

Figure 8.1. Fisher projection of the sidechain torsion angle χ_1 for residues Asp, Asn, Leu, Lys, Arg, Glu, Met, Pro, His, Phe, Tyr, and Trp. For Ala C^γ is substituted by $H^{\beta 1}$, for Ser C^γ is substituted by O^γ, and for Cys C^γ is substituted by S^γ. For Val C^γ is substituted by $C^{\gamma 1}$, $H^{\beta 2}$ by $C^{\gamma 2}$, and $H^{\beta 3}$ by H^β. For Thr C^γ is substituted by $C^{\gamma 2}$, $H^{\beta 2}$ by $O^{\gamma 1}$, and $H^{\beta 3}$ by H^β. Finally, for Ile C^γ is substituted by $C^{\gamma 2}$, $H^{\beta 2}$ by $C^{\gamma 1}$, and $H^{\beta 3}$ by H^β. Note that in accordance with IUPAC rules (IUPAC, 1970) the χ_1 torsion angle is defined by the orientation of the highest-ranking C^β substituent relative to the N-nucleus, and therefore differs for different residue types, e.g. Leucine vs *Threonine.*

constants, being ~2.5 and < 0.5 Hz for *trans* and *gauche* ^{3}J(NCγ), respectively, (Vuister et al., 1993a; Hu et al., 1997, Hu and Bax, 1997a) and ~3.0-4.0 and < 1.0 Hz for *trans* and *gauche* ^{3}J(C'Cγ), respectively (Grzesiek et al., 1993; Karimi-Nejad et al., 1994; Hu et al., 1997a,b).

Experiments aimed at measuring ^{3}J-coupling constants related to χ_2 are listed in Table 8.2. For most residues, only ^{3}J(HH), ^{3}J(CH), and ^{3}J(CC) coupling constants provide information about the χ_2 angle, although for selected residues also coupling constants involving other nuclei could be envisioned; e.g the sidechain carbonyl Cδ nucleus for Glu and Gln residues, or the Nδ nucleus for His residues.

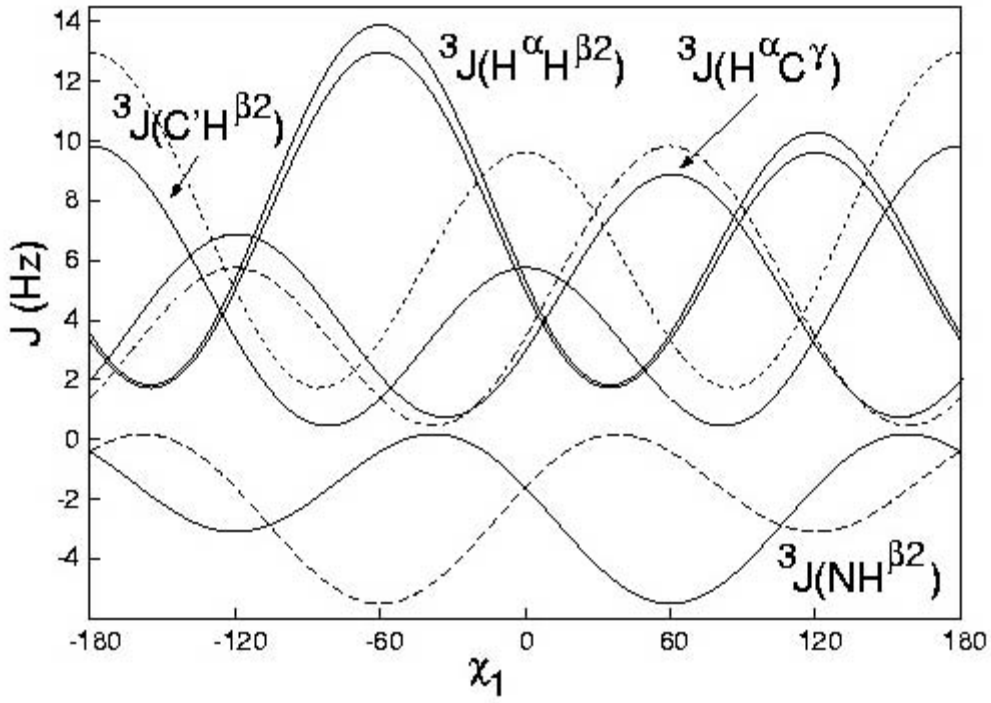

Figure 8.2. Karplus curves showing the dependencies of the $^3J(H^\alpha H^{\beta2})$, $^3J(H^\alpha H^{\beta3})$, $^3J(H^\alpha C^\gamma)$, $^3J(C'H^{\beta2})$, $^3J(C'H^{\beta3})$, $^3J(NH^{\beta2})$, and $^3J(NH^{\beta3})$ upon the torsion angle χ_1. The curves shown are: $^3J(H^\alpha H^{\beta2}) = 9.5\ cos^2(\chi_1\text{-}120°) - 1.68\ cos(\chi_1\text{-}120°) + 1.8$ (DeMarco et al., 1978a) and $^3J(H^\alpha H^{\beta2}) = 10.2\ cos^2(\chi_1\text{-}120°) - 1.8\ cos(\chi_1\text{-}120°) + 1.9$ (Bystrov, 1976) (solid thin line), $^3J(H^\alpha H^{\beta3}) = 9.5\ cos^2(\chi_1) - 1.68\ cos(\chi_1) + 1.8$ (DeMarco et al., 1978a) (dashed), $^3J(H^\alpha C^\gamma) = 7.1\ cos^2(\chi_1+120°) - 1.0\ cos(\chi_1+120°) + 0.7$ (Schmidt, 1997 and references therein), $^3J(C'H^{\beta2}) = 7.2\ cos^2(\chi_1) - 2.04\ cos(\chi_1) + 0.6$ (Fischman et al., 1980), $^3J(C'H^{\beta3}) = 7.2\ cos^2(\chi_1+120°) - 2.04\ cos(\chi_1+120°) + 0.6$ (Fischman et al., 1980) (short -long dashes), $^3J(NH^{\beta2}) = -4.4\ cos^2(\chi_1+120°) + 1.2\ cos(\chi_1+120°) + 0.1$ (DeMarco et al., 1978b), and $^3J(NH^{\beta3}) = -4.4\ cos^2(\chi_1\text{-}120°) + 1.2\ cos(\chi_1\text{-}120°) + 0.1$ (DeMarco et al., 1978b) (long dashes).

Table 8.1. Experiments for Measuring *J* Couplings Related to χ_1.

Coupling	Experiment[a]	References	Labeling	Remark
$^3J(H^\alpha H^\beta)$	E.COSY	Griesinger *et al.* (1986)	-	Original E.COSY
	HCCH COSY[H^β]	Gemmecker and Fesik (1991)	^{13}C	
		Griesinger and Eggenberger (1992)		
	HCCH TOCSY[H^β]	Gemmecker and Fesik (1991)	^{13}C	
		Emerson and Montelione (1992)		
	HXYH[H^β]	Tessari *et al.* (1995)	^{13}C	
	HAHB	Vuister *et al.* (1994)	^{12}C-reverse	
	HACAHB	Grzesiek *et al.* (1995)	^{13}C	
	CT-HACAHB	Tessari *et al.* unpublished	^{13}C	
$^3J(C'H^\exists)$	HN(CO)HB	Grzesiek *et al.* (1992)	$^{15}N/^{13}C$	
		Bax *et al.* (1994)		
	HNCACH-TOXSY[C´]	Weisemann *et al.* (1994b)	$^{15}N/^{13}C$	
$^3J(NH^\beta)$	NOESY[N]	Montelione *et al.* (1989)	^{15}N	
	HSQC-NOESY[N]	Wider *et al.* (1989)	^{15}N	
		Chary *et al.* (1991)		
	HNHB	Archer *et al.* (1991)	^{15}N	
		Madsen *et al.* (1993)		
		Düx *et al.* (1997)		Modified HNHB
	S^3E-sequence	Sorensen *et al.*, 1997		
$^3J(H^\alpha C^(')$	HMBC	Bax *et al.* (1988)	^{13}C	
	TOCSY	Zuiderweg en Fesik (1991)	^{13}C	Band-selective decoupling
	HMQC-TOCSY[C]	Edison *et al.* (1992)	Partial ^{13}C	
	LRCH	Vuister and Bax (1993b)	^{13}C	Val, Thr, Ile $C^(')H_3$
$^3J(NC^(')$	{^{15}N} sed[b] ^{13}C CT-HSQC	Vuister *et al.* (1993b)	$^{15}N/^{13}C$	Val, Thr, Ile $C^(')H_3$
	{$C^(')$} sed ^{15}N CT-HSQC	Hu *et al.* (1997)	$^{15}N/^{13}C$	Tyr, Phe, His, Trp
	HNCG	Hu and Bax (1997a)	$^{15}N/^{13}C$	
		Konrat *et al.* (1997)	$^{15}N/^{13}C$	
$^3J(C'C^(')$	{C´} sed ^{13}C CT-HSQC	Grzesiek *et al.* (1993)	$^{15}N/^{13}C$	Val, Thr, Ile $C^(')H_3$
	HCCCH-COSY[C´]	Schwalbe *et al.* (1993)	^{13}C	
	{$C^(')$} sed HNCO	Hu *et al.* (1997)	$^{15}N/^{13}C$	Tyr, Phe, His, Trp
		Konrat *et al.* (1997)	$^{15}N/^{13}C$	
$^3J(C'C'^(')$	HN(CO)CO	Hu and Bax (1996)	$^{15}N/^{13}C$	Asp and Asn

[a]Experiments are named analogous to the nomenclature proposed for triple-resonance experiments (Ikura *et al.* 1990). The passive spin in the E.COSY-type experiment is indicated in square brackets (Wang and Bax, 1995).

Table 8.2. Experiments for Measuring *J* Couplings Related to χ_2.

Coupling	Experiment[a]	References	Labeling	Remark
$^3J(HH)$	See Table 3 under $^3J(H^\alpha H^\beta)$			
$^3J(CH)$	HMBC	Bax *et al.* (1988)	^{13}C	
	HMQC-TOCSY[C]	Edison *et al.* (1992)	Partial ^{13}C	
	HSQC-TOCSY[C]	Sattler *et al.* (1992)	-	
	LRCH	Vuister *et al.* (1993b)	^{13}C-selective	
		Vuister and Bax (1993b)	^{13}C	Ile, Leu C^*H_3
$^3J(CC)$	LRCC	Bax *et al.* (1992, 1994)	^{13}C	Ile, Leu C^*H_3
	$HN(CO)CAC_{ali}$	Henning *et al.* (1997)	$^{15}N/^{13}C/^2H$	

[a]Experiments are named analogous to the nomenclature proposed for triple-resonance experiments (Ikura *et al.* 1990). The passive spin in the E.COSY-type experiment is indicated in square brackets (Wang and Bax, 1995).

9. Extracting the information

The magnitude of the ^{3}J-coupling constants can be correlated with the intervening dihedral angle through a Karplus equation (Karplus, 1959, 1963):

$$^3J = A\cos^2(\theta) + B\cos(\theta) + C \qquad (9.1)$$

Thus, the J-coupling can be translated into a structural restraint. The multi-valued nature of the Karplus equation, however, often requires information about a second J-coupling which is dependent upon the same torsion angle to resolve potential ambiguity. In case of rotameric averaging or prochiral groups, it is an absolutely necessity to obtain reliable information about several J-coupling constants. Alternatively, NOE information in conjunction with J-couplings can be used to establish stereospecific assignments and determine a rotameric state. Rather than using a rotatorial model for translating the J-value into a dihedral angle (cf. section 9.2), J-couplings can also be used in direct-refinement protocols using either a single-conformer J-value dependent potential or time- or ensemble-averaged J-value dependent potentials (Kim and Prestegard, 1990, Mierke et al., 1992,1994; Torda et al., 1993; Garrett et al., 1994).

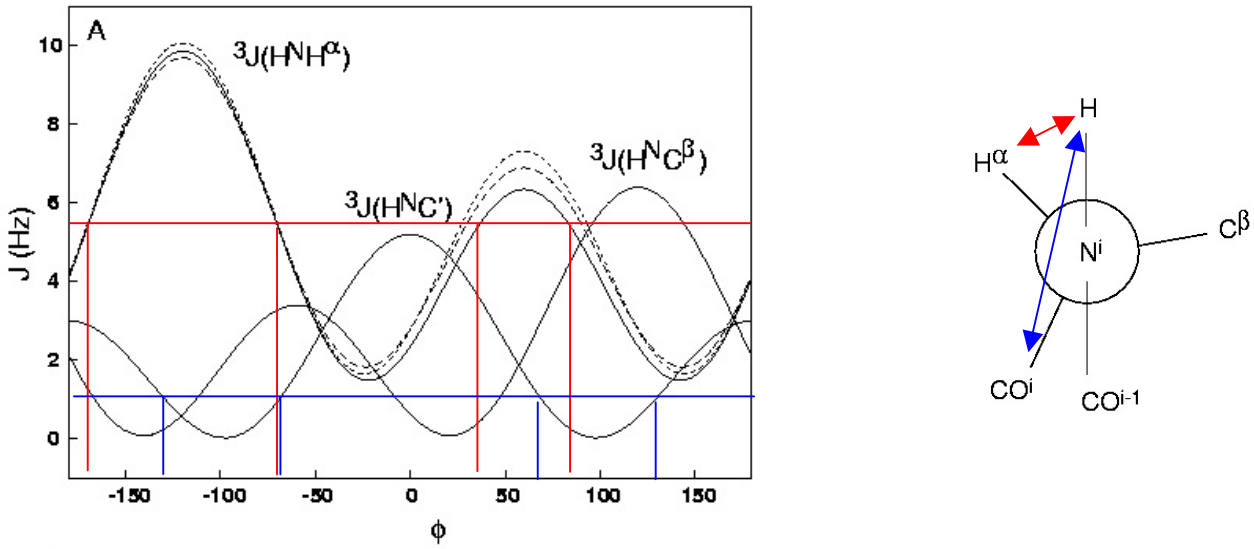

Figure 9.1. The multi-valued nature of the Karplus curve can be overcome by simultaneous analysis of several J-couplings. E.g. a $^3J(H^NH^\alpha)$ value of ~5.5 Hz yield to 4 solutions for ϕ. Only one of these (ϕ=-60) is compatible with a $^3J(H^NCO^{i-1})$ of ~1 Hz.

9.1. Parametrization of Karplus curves.

The accuracy of the appropriate Karplus curve is crucial to a meaningful interpretation of a measured J-value. The adjustable parameters of the Karplus curve, A, B, and C are traditionally have been determined by *ab initio* calculations or by studies on conformationally restricted small molecules (Bystrov, 1976). Alternatively, ^{3}J-values measured in proteins are compared with the dihedral angles found in the corresponding crystal structures (Pardi et al., 1984; Ludvigsen et al., 1991; Vuister and Bax, 1993a; Wang and Bax, 1995,1996; Hu et al., 1996; Hu and Bax, 1997b) or NMR-derived solution structures (Wang and Bax, 1996; Hu et al., 1997b). Since proper parametrization is of major importance for the interpretation of the ^{3}J-values (see Karimi-Nejad et al., 1994 for an example) it is useful to discuss some common sources of errors in the parametrization procedures.

The parametrization using small molecules is hampered by i) the usually low number of datapoints and ii) the differences in the electronic structure of the model compounds when compared to proteins. Consequently, in several instances parametrization of Karplus curves obtained from studies on small molecules yielded results which could not directly be used for the analysis of ^{3}J-values in proteins (Wang and Bax, 1995, 1996; Hu and Bax, 1996; Hu et al., 1997b).

Parametrization using ^{3}J-values measured in proteins is also complicated by serious difficulties, some of which are not easily overcome. The most common sources of errors are: i) The error in the measured ^{3}J-values. ii) The errors in the values of the dihedral angle θ. iii) When using dihedral angles derived from crystal structures: the genuine differences between crystal and solution structures, such as those caused by internal mobility in solution or those caused by distortions resulting from crystal contacts. iv) The limited range of accessable θ angles. v) The limited number of data points.

The experimental errors in the measured ^{3}J-values translate into errors in the parameters A, B, and C (cf. point i) above). Generally, there will be a range of values for the A, B, and C parameters which are in accordance with the experimental data. Some insight into this range can be obtained by a so-called jack-knife procedure. The A, B, and C parameters are usually determined by a least-squares fit of the measured ^{3}J-values versus θ (using some error estimate for the ^{3}J-value). If however, arbitrarily 10% of the measured values are omitted and the A, B, and C parameters are determined again, slightly different values are obtained. The remaining 10% of the data can be used

to assess the error. Repetition of this procedure for different randomly chosen sets of 10% deletion yields a range of accessible parameters. An example of this is shown in Figure 9.2 for the parametrization of the $^3J(H^NH\alpha)$ coupling constant on the basis of the $^3J(H^NH\alpha)$ values measured for staphylococcal nuclease using the HNHA experiment (Vuister and Bax, 1993a).

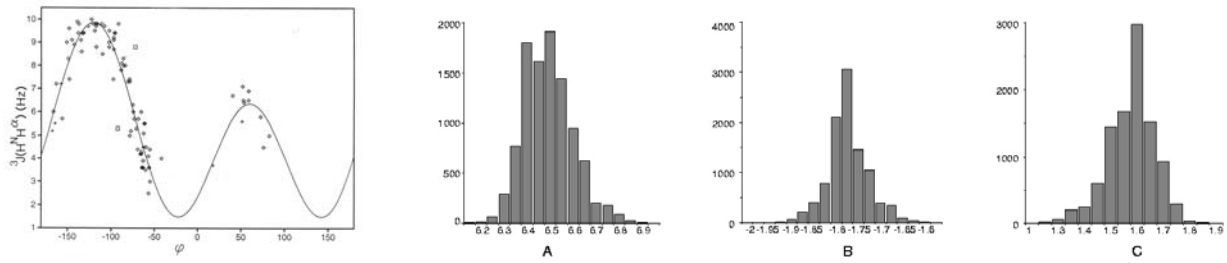

Figure 9.2. Experimental $^3J(H^NH\alpha)$ values versus ϕ(crystal structure) of Snase and Karplus curve. Histograms of the A, B, and C parameters of the obtained by a 'jackknife procedure' (data from Vuister and Bax, 1993a).

Errors resulting from point ii) mentioned above, could be minimized by using only high-resolution crystal structures, preferentially in several crystal forms. Differences between solution and NMR structures (cf. point iii) above) can be assessed by careful comparison. The problem associated with point iv) needs particular attention if ^3J-values are analysed which significantly fall outside the range used for parametrization. Also conclusions pertaining to dihedral angle values which have not been sampled in the parametrization process should be evaluated with great care. The rapidly expanding database of ^3J-values should improve the errors resulting from point v).

9.2. Analysis of J-couplings in Proteins.

When analysing ^3J-coupling constants in proteins, their translation into the corresponding dihedral angles is hampered by two different problems: First, the Karplus equation is not a single-valued function in a mathematical sense, yielding up to four dihedral angle values for a given ^3J-value. Therefore, in order to obtain an unambiguous answer it is necessary to determine a set of coupling constants related to the same torsion angle in the protein. Second, conformational mobility, especially encountered in protein side chains, may lead to coupling constants that are averages over multiple conformations (Pople, 1958; Hoch et al., 1985). In these cases, the observed time-averaged coupling constant is given by:

$$\langle J \rangle = \int_{-\pi}^{\pi} J(\theta)\, P(\theta) d\theta \tag{8.2}$$

where P(θ) is the probability to observe the value J(θ) for the torsion angle θ at a given temperature T according to:

$$P(\theta) = \frac{e^{-E(\theta)/kT}}{\int_{-\pi}^{\pi} e^{-E(\theta)/kT} d\theta} \tag{9.3}$$

and E(θ) defines the torsional potential. If all possible values of θ have the same probability, i.e. if complete rotational averaging occurs, P(θ) = 1/2[1] and one obtains according to eqs. 8.1 and 8.2 an average coupling constant from the Karplus relationship:

$$\langle {}^3J \rangle = A / 2 + C \tag{9.4}$$

Only if E(θ), which depends on the intrinsic dihedral potential as well as on the environment (e.g. the solvent or the protein matrix) of the torsion angle under consideration would be known, rotameric probability distributions as well as coupling constant values could be predicted. Since this is usually not the case, one has to set up suitable models for the description of rotatorial mobility.

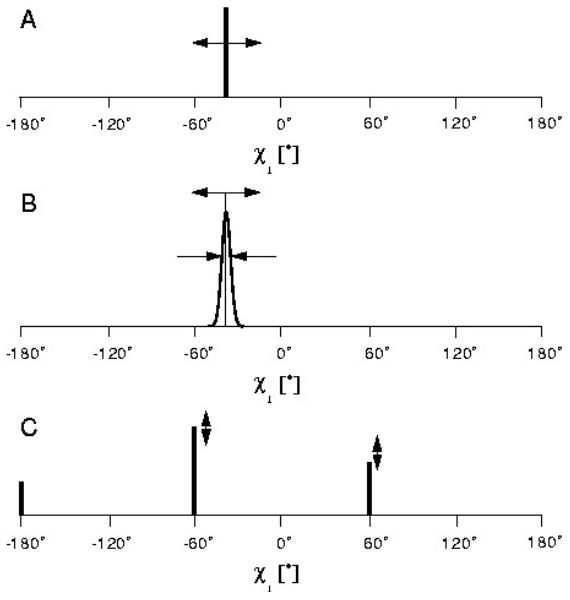

Figure 9.3. Models of rotatorial mobility (adapted from Schmidt, 1997): single-site model (A), gaussian distribution (B), and staggered rotamers (C).

9.2.1. Models of rotatorial mobility.

In the simple single-site model (cf. Fig. 9.3A) the experimental value, J^{exp}, is explained by assuming a fixed dihedral angle, θ:

$$J^{exp} = J^{calc}(\theta) \tag{9.5}$$

where $J^{calc}(\theta)$ is derived from the appropriate Karplus curve. The model has only one adjustable parameter, i.e. θ.

The second model assumes a unimodal Gaussian distribution, where the angle θ is allowed to fluctuate about an expectation value, $\langle\theta\rangle$, with a given width, σ_θ, (cf. Fig. 9.3B) resulting in a two-parameter model according to:

$$J^{exp} = J^{calc}(\langle\theta\rangle,\sigma_\theta) = \frac{1}{\sigma_\theta\sqrt{2\pi}} \int_{-\pi}^{\pi} J^{calc}(\theta) e^{-\frac{1}{2}\left(\frac{\theta-\langle\theta\rangle}{\sigma_\theta}\right)^2} d\theta \tag{9.6}$$

Traditionally, and especially in the case of peptide side chains, the Pachler analysis (Pachler, 1963,1964) (cf. Fig. 9.3C) has found widespread use for the interpretation of motionally averaged coupling constants, assuming conformational equilibria between discrete staggered rotamers, e.g. the side chain angle χ_1 (Kessler et al., 1987). The populations of these staggered rotamers, p_I, p_{II}, and p_{III}, of the sites with θ = 180°, -60°, and +60°, respectively, are allowed to vary to obtain the closest correspondence between experimentally derived J-couplings and values back-calculated from the model. The resulting model is described by two independent adjustable parameters:

$$J^{exp} = J^{calc}(p_I, p_{II}, p_{III}) = p_I J^{calc}(\theta = 180°) + p_{II} J^{calc}(\theta = -60°) + p_{III} J^{calc}(\theta = 60°) \tag{9.7a}$$

$$p_I + p_{II} + p_{III} = 1 \tag{9.7b}$$

Possible limitations of this model arise from the assumption of a three-fold torsion potential with minima at θ = -60°, +60°, and 180° that might not always be correct (Gelin and Karplus, 1979; Fischman et al., 1980; Schrauber et al., 1993).

Continuous dihedral-angle distributions have also been used to describe the rotatorial dynamics of protein side chains, both to explain theoretical coupling constant data derived from

solvated MD simulations (Hoch et al., 1985; Brüschweiler and Case, 1994) as well as to fit experimental data (Dzakula et al., 1992 a,b; Karimi-Nejad et al., 1994).

10. Conclusions

1. ^{3}J values can now be measured fairly routinely in biomolecules.
2. ^{3}J values provide useful information at modest 'costs'.
3. ^{3}J values provide information about dynamics.
4. ^{3}J values can provide an independent parameter for validation of the quality of the structure.
5. ^{1}J and ^{2}J values can be measured using similar techniques

11. Practical Outline

Stage 1: Extracting initial information

1. Backbone angle ϕ: HNHA (HNCA[H^{α}]), HN(CO)CO.
2. Backbone angle ψ: shifts (Talos), (cross-correlated relaxation).
3. Sidechain angle χ_1: SED experiments Val, Thr, Ile $C^{\gamma}H_3$, aromatics
4. Sidechain angle χ_2: LRCC Leu, Ile $C^{\delta}H_3$

Stage 2: Extracting additional information for complete analysis

1. Remaining experiments
2. Deuteration: Griesinger et al. (1998) p304

12. References related to measurement of RDCs

Fundamentally, there is no difference when measuring J-couplings with the aim to extract RDCs. Hence, the same type of techniques are used such as enhancing schemes, frequency domain methods, IPAP, Quantitative J methods, and E.COSY methods. However, there are special consideration to consider such as the typically greater variability of the measured values, the presence of interfering effects such as ^{1}H-^{1}H RDCs, and relaxation effects.

The following papers may help you get started:

Reviews

- Prestegard et al., "NMR structures of biomolecules using field oriented media and residual dipolar couplings", Quarterly Rev. Biophys. 33, 371-424 (2000).
- Bax et al, "Dipolar couplings in macromolecular structure determination", Meth. Enzymol. 339, 127-174 (2001).
- Alba & Tjandra, "NMR dipolar couplings for the structure determination of biopolymers in solution", Prog. Nucl. Magn. Reson. 40, 175-197 (2002).

Others

- Lerche et al, "Pulse sequences for measurement of one-bond 15N-1H couplings in the protein backbone", J. Magn. Reson. 140, 259-263 (1999).
- Kontaxis et al., "Evaluation of cross-correlation effects and measurment of –one-bond ouplings in proteins with short transverse relaxation times", J. Magn. Reson. 143, 184-196 (2000).
- Chou et al., "Measurement of one-bond 15N-13C' dipolar couplings in medium sized proteins", J. Biomol. NMR, 18, 101-105 (2000).
- Wu & Bax, "Measurement of long-range ^{1}H-^{1}H dipolar couplings in weakly aligned proteins", J. Am. Chem. Soc. 124, 9672-9673 (2002).
- Cutting et al., "Accurate measurement of residual dipolar couplings in anisotropic phase", J. Biomol. NMR, 23, 195-200 (2002).
- Wienk et al., "Simultaneous measurement of protein one-bond and two-bond nitrogen-carbon coupling constants using an internally referenced quantitative J-correlated [^{15}N,^{1}H]-TROSY-HNC experiment", J. Biomol. NMR 25, 133-145 (2003).

13. References

Archer, S.J., Ikura, M., Torchia, D.A., and Bax, A., 1991, *J. Magn. Reson.* **95**: 636.

Bax, A., and Freeman, R., 1981a, *J. Magn. Reson.* **44**: 542.

Bax, A., and Freeman, R., 1981b, *J. Magn. Reson.* **45**: 177.

Bax, A., Sparks, S.W., and Torchia, D.A., 1988, *J. Am. Chem. Soc.* **110**:7926.

Bax, A., Max, D., and Zax, D., 1992, *J. Am. Chem. Soc.* **114**: 6924.

Bax, A., Vuister, G.W., Grzesiek, S., Delaglio, F., Wang, A.C., Tschudin, R., and Zhu, G., 1994, Measurement of homo- and heteronuclear J couplings from quantative J correlation, in Methods in Enzymology **239** (T.L. James & N.J. Oppenheimer, eds.), Academic Press, San Diego, pp. 79-105.

Billeter, M., Neri, D., Otting, G., Qiu Qian, Y., and Wüthrich, K., 1992, *J. Biomol. NMR* **2**: 257.

Blake, P.R., Summers, M.F., Adams, M.W.W., Park, J.-B., Zhou, Z.H., and Bax, A., 1992, *J. Biomol. NMR* **2**: 527.

Brüschweiler, R., and Case, D., 1994, *J. Am. Chem. Soc.* **116**: 11199.

Bystrov, V.F., 1976, *Prog. NMR Spectrosc.* **10**: 41.

Chary, K.V.R., Otting, G., and Wüthrich, K., 1991, *J. Magn. Reson.* **93**: 218.

Delaglio, F., Torchia, D.A., and Bax, A., 1991, *J. Biomol. NMR* **1**: 439.

DeMarco, A., Llinas, M., and Wüthrich, K., 1978a, *Biopolymers* **17**: 617.

DeMarco, A., Llinas, M., and Wüthrich, K., 1978b, *Biopolymers* **17**: 2727.

Dzakula, Z, Westler, W.M., Edison, A.S., Markley, J.L., 1992a, *J. Am. Chem. Soc.* **114**: 6195.

Dzakula, Z., Edison, A.S., Westler, W.M., Markley, J.L., 1992b, *J. Am. Chem. Soc.* **114**: 6200.

Düx, P., Whitehead, B., Boelens, R., Kaptein, R., and Vuister, G.W., 1997a, *J. Biomol. NMR* **1**0:301.

Düx, P., Rubinstenn, G., Vuister, G.W., Boelens, R., Mulder , F.A.A., Hård, K., Hoff, W.D., Kroon, A., Hellingwerf, K.J., and Kaptein, R., 1997b, *Biochemistry* **37**:12689.

Edison, A.S., Westler, W.M., and Markley, J.L., 1992, *J. Magn. Reson.* **92**: 434.

Eggenberger, U., Karimi-Nejad, Y., Thüning, H., Rüterjans, H., and Griesinger, C., 1992, *J. Biomol. NMR* **2**: 583.

Emerson, S.D., and Montelione, G.T., 1992, *J. Magn. Reson.* **99**: 413.

Fischman, A.J., Live, D. H., Wyssbrod, H.R., Agosta, W.C., and Cowburn, D., 1980, *J. Am. Chem. Soc.* **102**: 2533.

Garrett, D.S., Kuszewski, J., Hancock, T.J., Lodi, P.J., Vuister, G.W., Gronenborn, A.M., and Clore, G.M., 1994, *J. Magn. Reson. B* **104**: 99.

Gelin, B.R., and Karplus, M., 1979, *Biochemistry* **18**: 1256.

Gemmecker, G., and Fesik, S.W., 1991, *J. Magn. Reson.* **95**: 208.

Görlach, M., Wittekind, M., Farmer II, B.T., Kay, L.E., and Mueller, L., 1993, *J. Magn. Reson. B* **101**: 194.

Griesinger, C., Sörensen, O.W., and Ernst, R.R., 1985, *J. Am. Chem. Soc.* **107**: 6394.

Griesinger, C., Sörensen, O.W., and Ernst, R.R., 1986, *J. Chem. Phys.* **85**: 6837.

Griesinger, C., Sörensen, O.W., and Ernst, R.R., 1987, *J. Magn. Reson.* **75**: 474.

Griesinger, C., and Eggenberger, U., 1992, *J. Magn. Reson.* **97**: 426.

Griesinger, C., Hennig, M., Marino, J.P., Reif, B., Richter, C. and Swalbe, H., 1998, in Biological Magnetic Resonance 16. "Modern Techniques in protein NMR" eds. N.Rama Krishna and Lawrence J. Berliner, 1998, (Kluwer Academic/Plenum Publishers) p259-367.

Grzesiek, S., Ikura, M., Clore, G.M., Gronenborn, A.M., Bax, A., 1992, *J. Magn. Reson.* **96**: 215.

Grzesiek, S., Vuister, G.W., and Bax, A., 1993, *J. Biomol. NMR* **3**: 487.

Grzesiek, S., Kuboniwa, H., Hinck, A.P., and Bax, A., 1995, *J. Am. Chem. Soc.* **117**: 5312.

Haasnoot, C.A.G., de Leeuw, F.A.A.M., and Altona, C., 1980, *Tetrahedron Lett.* **36**: 2783.

Hennig, M., Ott, D., Schulte, P., Lšwe, R., Krebs, J., Vorherr, T., Bermel, W., Schwalbe, H., and Griesinger, C., 1997, *J. Am. Chem. Soc.* **119**: 5055.

Hoch, J.C., Dobson, C.M., and Karplus, M., *Biochemistry* **24**: 3831.

Hu, J.-S., and Bax, A., 1996, *J. Am. Chem. Soc.* **118**: 8170.

Hu, J.-S., and Bax, A., 1997a, *J. Biomol. NMR* **9**: 323.

Hu, J.-S., and Bax, A., 1997b, *J. Am. Chem. Soc.* **119**: 6360.

Hu, J.-S., Grzesiek, S., and Bax, A., 1997, *J. Am. Chem. Soc.* **119**:1803.

IUPAC, 1970, *Biochemistry* **9**: 3471.

Ikura, M., Kay, L.E., and Bax, A., 1990, *Biochemistry* **29**: 2577.

Karimi-Nejad, Y., Schmidt, J. M., RŸterjans, H., Schwalbe, H., and Griesinger, C., 1994, *Biochemistry* **33**: 5481.

Karimi-Nejad, Y., 1996, *NMR-spektroskopische Untersuchungen zur Struktur der Ribonuclease T1 und ihrer Komplexe mit 2Õ- und 3Õ- Guanosinmonophosphat*, Thesis, UniversitŠt Kšln.

Karplus, M., 1959, *J. Chem. Phys.* **30**: 11.

Karplus, M., 1963, *J. Am. Chem. Soc.* **85**: 2870.

Kay, L.E., Brooks, B., Sparks, S.W., Torchia, D.A., and Bax, A., 1989, *J. Am. Chem. Soc.* **111**: 5488.

Kay, L.E., and Bax, A., 1990, *J. Magn. Reson*. **86**: 110.

Kay, L.E., Keifer, P., and Saarinen, T., 1992, *J. Am. Chem. Soc.* **114**: 10663.

Kessler, H., Griesinger, C., and Wagner, K., 1987, *J. Am. Chem. Soc.* **109**: 6927.
Kim, Y., and Prestegard, J.H., 1990, *Proteins: Struct. Func. Genet.* **8**: 377.
Konrat, R., Muhandiram, D. R., Farrow, N. A., and Kay, L. E., 1997. *J. Biomol Nmr* **9**, 409.
Kuboniwa, H., Grzesiek, S., Delaglio, F., and Bax, A., 1994, *J. Biomol. NMR* **4**: 871.
Löhr, F,. and Rüterjans, H., 1995, *J. Biomol. NMR* **5**: 25.
Löhr, F,. and Rüterjans, H., 1997, *J. Am. Chem. Soc.* **119**: 1468.
Löhr, F., Blumel, M., Schmidt, J. M, and Rüterjans, H.,1997, *J Biomol Nmr* **10**: 107.
Lohr, F. and Ruterjans, H., 1999, *J Biomol Nmr* **13**:263 .
Ludvigsen, S., Andersen, K.V., and Poulsen, F.M., 1991, *J. Mol. Biol.* **217**: 731.
Madsen, J.C., S¿rensen, O.W., S¿rensen, P., and Poulsen, F.M., 1993, *J. Biomol. NMR* **3**: 239.
Mierke, D.F., Grdadolnik, S.G., and Kessler, H., 1992, *J. Am. Chem. Soc.* **114**: 8283.
Mierke, D.F., Huber, T., and Kessler, H., 1992, *J. Comp. Aided Mol. Design* **8**: 29.
Montelione, G.T., Winkler, M.E., Rauenbuehler, P., and Wagner, G. , 1989, *J. Magn. Reson.* **82**: 198.
Madsen, J.C., S¿rensen, O.W., S¿rensen, P., and Poulsen, F.M., 1993, *J. Biomol. NMR* **3**: 239.
Neri, D., Otting, G., and WŸthrich, K., 1990, *J. Am. Chem.ÊSoc.* **112**: 3663.
Otting, G., 1997, *J. Magn. Reson.* **124**: 503.
Pachler, K.G.R., 1963, *Spectrochim. Acta* **19**: 2085.
Pachler, K.G.R., 1964, *Spectrochim. Acta* **20**: 581.
Palmer, A.G., Cavanagh, J., Wright, P.E., and Rance, M., 1991, *J. Magn. Reson.* **93**: 151.
Pardi, A., Billeter, M., and WŸthrich, K., 1984, *J. Mol. Biol.* **180**: 741.
Ponstingl, H. and Otting, G., 1998, *J Biomol Nmr* **12**:319.
Rexroth, A., Szalma, S., Weisemann, R., Bermel, W., Schwalbe, H., and Griesinger, C., 1995a, *J. Biomol. NMR* **6**: 237.
Rexroth, A., Schmidt, P., Szalma, S., Geppert, T., Schwalbe, H., and Griesinger, C., 1995b, *J. Am. Chem. Soc* **117**: 10389.
Pople, J.A., 1958, *Mol. Phys.* **1**: 3.
Sattler, M., Schwalbe, H., and Griesinger, C., 1992, *J. Am. Chem. Soc.* **114**: 1126.
Schmidt, J., 1997, *J. Magn. Reson.* **124**: 310.
Schmieder, P., Thanabal, V., McIntosh, L.P., Dahlquist, F.W., and Wagner, G., 1991, *J. Am. Chem. Soc.* **113**: 6323.
Schrauber, H., Eisenhaber, F., and Argos, F., 1993, *J. Mol. Biol.* **230**: 592.
Schwalbe, H., Marino, J.P., King, G.C., Wechselberger, R., Bermel, W., and Griesinger, C., 1994, *J. Biomol. NMR* **4**: 631.
Sörensen, O.W., 1990, *J. Magn. Reson.* **90**: 433.
Sörensen, M. D., Meissner, A., and Sörensen, O. W., 1997, *J Biomol Nmr* **10**:181
Seip, S., Balbach, J., and Kessler, H., 1992, *Angew. Chem. Int. Ed. Engl.* **31**: 1609.
Seip, S., Balbach, J., and Kessler, H., 1994, *J. Magn. Reson. B* **104**: 172.
Schwalbe, H., Rexroth, A., Eggenberger, U., Geppert, T., and Griesinger, C., 1993, *J. Am. Chem. Soc.* **115**: 7878.
Tessari, M., Mariani, M., Boelens, R., and Kaptein, R., 1995, *J. Magn. Reson. B* **108**: 89.
Theis, K., Dingley, A. J., Hoffmann, A., Omichinski, J. G., and Grzesiek, S. , 1998, *J Biomol Nmr* **10**:403.
Torda, A.E., Brunne, R.M., Huber, T., Kessler, H., and van Gunsteren, W.F., 1993, *J. Biomol. NMR* **3**: 55.
Vuister, G.W., and Bax, A., 1992, *J. Biomol. NMR* **2**: 401.
Vuister, G.W., and Bax, A., 1993a, *J. Am. Chem. Soc.*, **115**: 7772.
Vuister, G.W., and Bax, A., 1993b, *J. Magn. Reson. B* **102**:228.
Vuister, G.W., Wang, A.C., and Bax, A., 1993a, *J. Am. Chem. Soc.* **115**: 5334.
Vuister, G.W., Yamazaki, T., Torchia, D.A., and Bax, A., 1993b, *J. Biomol. NMR* **3**: 297.
Vuister, G.W., and Bax, A., 1994, *J. Biomol. NMR* **4**: 193.
Vuister, G.W., Kim, S.-J., Wu, C., and Bax, A., 1994, *J. Am. Chem. Soc.* **116**: 9206.
Vuister, G.W., Tessari, M., Karimi-Nejad, Y., Whitehead, B., 1998, in Biological Magnetic Resonance, Vol. 16: Modern Techniques in Protein NMR, edited by Krishna and Berliner, Kluwer Academic/Plenum Publishers.
Wang, A.C., and Bax, A., 1995, *J. Am. Chem. Soc.*, **117**: 1810.
Wang, A.C., and Bax, A., 1996, *J. Am. Chem. Soc.*, **118**: 2483.
Weisemann, R., Rüterjans, H., Schwalbe, H., Schleucher, J., Bermel, W., and Griesinger, C., 1994a, *J. Biomol. NMR* **4**: 231.
Weisemann, R., Löhr, F., and Rüterjans, H., 1994b, *J. Biomol. NMR* **4**: 587.
Wider, G., Neri, D., Otting, G., and Wüthrich, K., 1989, *J. Magn. Reson.* **85**: 426.
Zuiderweg, E.R.P, and Fesik, S.W., 1991, *J. Magn. Reson.* **93**: 653.